Structural controls on the location, geometry, and longevity of an intraplate volcanic system – The Tuatara Volcanic Field, Great South Basin, New Zealand

[1]*Thomas B. Phillips & [2]Craig Magee

[1]*Department of Earth Sciences, Durham University, Science Labs, Elvet Hill, Durham, DH13LE*

[2]*Institute of Geophysics and Tectonics, School of Earth Science and Environment, University of Leeds, Leeds, LS2 9JT, UK*

**Corresponding Author – thomas.b.phillips@durham.ac.uk*

Abstract

Intraplate volcanism is widely distributed across continental interiors. Yet controls on the location, 3D geometry, and longevity of many individual intraplate volcanic systems are often poorly understood. Geophysical and geodetic data provide insights into active intraplate magma plumbing systems, particularly when coupled with petrological and chemical analyses of volcanic products, but these techniques are relatively low resolution and reveal little about the host rock structure. It is therefore difficult to evaluate whether magma transiting the lithosphere is directed by the complex and highly heterogeneous structure of continental interiors. Here, we use borehole-constrained 2D seismic reflection data to characterise the 3D geometry of the newly-discovered, ancient, intraplate Tuatara Volcanic Field in the Great South Basin, offshore the South Island of New Zealand, and investigate its relationship with pre-existing crustal and lithospheric structures. The ~270 km^2 Tuatara Volcanic Field is dominated by a dome-shaped edifice of tabular lavas, surrounded and overlain by ~69 distinct volcanoes connected and likely fed by a network of >70 sills. Seismic-stratigraphic analyses reveal

the volcanic system developed over 40 Myr, between the Late Cretaceous and Early Eocene (~85 Ma–45 Ma). We find that the Tuatara Volcanic Field is located directly above the Livingstone Fault, which separates the Caples and Dun Mountain-Maitai basement terranes; the recently active (600 yr before present) Auckland Volcanic Field is similarly located above the Livingstone Fault along-strike on the North Island. We suggest the Livingstone Fault controlled the location of the Tuatara Volcanic Field by: (i) producing relief at the base lithosphere, which we propose focused small-scale convection and/or lithosphere detachment, promoting periodic melting over ~40 Myr; and (ii) providing a pathway that facilitated magma ascent. Our work highlights that (recently) active intraplate volcanic systems, including the Auckland Volcanic Field, may comprise distributed volcanoes interconnected by sill-complexes, and be spatially and temporally controlled by pre-existing crustal and/or lithospheric structures.

1 Introduction

Intraplate volcanism encompasses igneous activity away from and unrelated to plate boundary processes (e.g. subduction and mid-ocean ridge spreading). Such intraplate volcanic systems develop in a variety of forms, from the construction of volcanic chains (e.g., Davies et al., 2015), through to large caldera forming eruptions (e.g., Timm et al., 2009) or the formation of volcanic fields comprising small, relatively short-lived volcanoes (e.g., Németh, 2010; Németh et al., 2003; Reynolds et al., 2018). These different styles of volcanic activity reflect the range of processes that drive, and influence the location and longevity of, intraplate volcanism. For example, hotspot intraplate volcanism occurs above a fixed, thermal mantle anomaly, producing chains of extinct volcanoes as plate motion carries active volcanoes away from the melt source (e.g. Clague and Jarrard, 1973; Morgan, 1972; Sleep, 1992). In contrast, during continental rifting, the location and longevity of intraplate volcanic systems relates to the location and magnitude of lithospheric thinning (e.g., Wilson et al., 1995; Wu et al., 2018). In other intraplate settings, such as the Turkish-Iranian Plateau, Eastern Australia, or Zealandia, diffuse volcanism occurs seemingly randomly over wide (continental-scale) areas (e.g., Finn et al., 2005; Hoernle et al., 2006; Kaislaniemi et al., 2014; Rawlinson et al., 2017). Whilst records of intraplate volcanism across these broad areas may be relatively continuous,

individual volcanic systems are typically active across much shorter (Myr) timescales. Relative to hotspot- or rift-related intraplate volcanism, the processes driving the formation of these diffuse volcanic fields are often elusive and we particularly poorly understand the factors controlling the distribution and longevity of individual volcanic systems (e.g. Valentine and Hirano, 2010). In the absence of a clear process-driven control on the distribution of intraplate volcanic fields, pre-existing lithospheric and/or crustal structures may represent a crucial and commonly overlooked influence on their siting, magma plumbing system structure, and longevity.

Constraining the 3D geometry of magma plumbing systems and assessing how intraplate volcanism relates to and/or may be influenced by pre-existing structures is difficult because (see Magee et al., 2018 and references therein): (i) geophysical and geodetic data typically provide only a relatively low resolution view of subsurface magma or igneous rock distribution, and capture little information on host rock structure; (ii) outcrop analyses of ancient plumbing systems allow detailed analyses of intrusion geometry and host rock structure, but limitations in exposure at Earth's surface mean we cannot often place these observations within a 3D context; and (iii) petrological and chemical data, whilst providing crucial insights into melt and magma evolution, are often interpreted within a poorly defined structural framework. Reflection seismology provides a powerful tool for imaging the 3D geometry of volcanoes and magma plumbing systems in the subsurface (e.g., Bischoff et al., 2017; Buntin et al., 2019; Magee et al., 2019; Magee et al., 2016; McLean et al., 2017; Morley, 2018; Quirie et al., 2019; Reynolds et al., 2017; Sun et al., 2019a).

Here, we use borehole-constrained seismic reflection data to investigate the 3D structure of a hitherto unidentified intraplate volcanic field buried within the Great South Basin, offshore of the South Island of New Zealand. The volcanic field comprises a ~270 km^2 central edifice, formed of stacked lavas, surrounded and overlain by 69 volcanic cones; we also identify a network of >70 igneous sills that formed the shallow-level plumbing system and linked to individual volcanoes. We name this newly discovered province the 'Tuatara Volcanic Field' after the endemic New Zealand reptile, the name of which is derived from the Māori language and fittingly means 'peaks on the back'. The well exposed and studied basement geology onshore New Zealand (e.g., Mortimer, 2004; Tarling et al., 2019),

77 combined with a detailed and comprehensive record of intraplate volcanism throughout the Cenozoic
78 (e.g., Adams, 1983; Cooper et al., 1987; Hoernle et al., 2006; Németh and White, 2003; Rout et al.,
79 1993; Speight, 1943; Stipp and McDougall, 1968; Waight et al., 1998) and high-resolution marine
80 geological and geophysical data available in the offshore domain (e.g., Mortimer et al., 2002; Phillips
81 and McCaffrey, 2019; Tulloch et al., 2019; Uruski, 2015; Uruski et al., 2007), allow us to fully
82 characterise and constrain the internal architecture of the Tuatara Volcanic Field and assess how it
83 relates to the surrounding crustal structure. By identifying seismic-stratigraphic onlap and downlap
84 relationships, we show the volcanoes and sills were emplaced between ~85 and ~45 Ma, recording
85 ~40 Myr of punctuated igneous activity spanning the Late Cretaceous-to-Early Eocene.

86 We propose the location and longevity of the Tuatara Volcanic Field was controlled by the underlying
87 terrane boundary marked by the Livingstone Fault. In particular, we suggest changing relief of the
88 lithosphere-asthenosphere boundary across the terrane boundary promoted local lithospheric
89 detachment and melting, whilst the Livingstone Fault facilitated magma ascent. The structural setting
90 of the Tuatara Volcanic Field is equivalent to that of the recently active Auckland Volcanic Field on
91 the North Island (active 30 Ka - 600 y BP; Lindsay et al., 2011). Our study of the Tuatara Volcanic
92 Field, which highlights the roles of pre-existing structure and sill-complex development in controlling
93 the location and longevity of volcanic activity, may offer important insights into the processes
94 occurring at the Auckland Volcanic Field and intraplate volcanism elsewhere.

95

96 2 Geological setting

97 Zealandia is an ideal natural laboratory to explore how crustal structure may affect the distribution,
98 geometry, and evolution of volcanic fields: it hosts a long record of intraplate volcanism, from the
99 Cenozoic to present day, dispersed across the length and breadth of a continent comprising a
100 heterogeneous basement formed of multiple distinct terranes (e.g., Mortimer, 2004; Mortimer et al.,
101 2002; Mortimer et al., 1999; Phillips and McCaffrey, 2019; Tulloch et al., 2019). This study focusses
102 on a ~10,000 km^2 area in the northern part of the Great South Basin, offshore the east coast of the

South Island of New Zealand and located 60 km SE of the Dunedin Volcano on the Otago Peninsula (Figure 1). The study area forms part of the Campbell Plateau on the continental shelf of Zealandia, an extensive area of submerged and extended continental crust characterised by water depths of ~500–1500 m (Adams, 1962).

2.1 Regional geological evolution

The basement geology of New Zealand comprises the Austral Superprovince, which incorporates a series of terranes that accreted along the southern margin of Gondwana during Cambrian-to-Cretaceous subduction (e.g., Bishop et al., 1985; Howell, 1980; Johnston, 2019; Mortimer, 2004; Mortimer et al., 2014). These terranes are divided into the Eastern and Western provinces, which are separated by the Median Batholith (Figure 1) (Mortimer, 2004; Mortimer et al., 1999). Projecting onshore terrane boundaries offshore along-strike suggests the study area resides within the Eastern Province and spans the faulted boundary between the Caples Terrane and the Dun Mountain-Maitai Terrane (Figure 1). This terrane boundary corresponds to the Livingstone Fault (Figure 1), which is a serpentinite-dominated shear zone that ranges from 10's to 100's of metres wide, dips steeply to the northeast, and extends down to, at least, the base of the crust (Mortimer et al., 2002; Tarling et al., 2019). The Caples Terrane comprises weakly metamorphosed volcaniclastic greywackes, which accreted to the southern margin of Gondwana during the Permian-to-Triassic (Johnston, 2019; Mortimer, 2004; Robertson et al., 2019), whilst the Dun Mountain-Maitai Terrane includes the Early Permian Dun Mountain, mafic-to-ultramafic ophiolite belt and an overlying, 6 km thick sequence of Late Permian-Middle Triassic volcaniclastic sedimentary rocks (i.e. the Maitai Group; Mortimer, 2004). Due to its mafic/ultramafic lithology, the Dun Mountain ophiolite is delineated by the Junction Magnetic Anomaly, which forms a ~20 km wide positive anomaly onshore (e.g.,Davey and Christoffel, 1978; Sutherland, 1999; Tulloch et al., 2019), but is less prominent offshore (Figure 2). Further positive magnetic anomalies, forming part of the Stokes Magnetic Anomaly System, are identified south of the Junction Magnetic Anomaly and likely relate to the Rotoroa igneous province and additional volcanics within the Eastern Province terranes (Figure 2) (Grobys et al., 2009; Hunt, 1978; Sutherland, 1999; Woodward and Hatherton, 1975).

Subduction and terrane accretion along the southern margin of Gondwana ceased during the mid-to-late Cretaceous as the Hikurangi Plateau, part of a Large Igneous Province, collided with and jammed the subduction zone (Davy et al., 2008). Following the cessation of subduction, Zealandia underwent two major phases of rifting related to the breakup of Gondwana during the Late Cretaceous (Figure 1B) (Kula et al., 2007; Laird and Bradshaw, 2004; Mortimer et al., 2019; Tulloch et al., 2019; Uruski et al., 2007). Initial rifting from ~100–90 Ma related to break-up between Zealandia and Australia, and may have led to extensional reactivation of terrane boundaries beneath the proto-Great South Basin (Figure 1) (Phillips and McCaffrey, 2019). The second rift phase occurred from ~90–80 Ma in response to extension between Zealandia and Western Antarctica, resulting in the formation of the NE-trending Great South and Canterbury basins (Figure 1) (Beggs, 1993; Grobys et al., 2009; Kula et al., 2007; Tulloch et al., 2019).

The Alpine Fault formed during the Early Cenozoic to accommodate plate motion between the Pacific and Australian plates. Although located relatively close (~200 km) to the Alpine Fault between the Pacific and Australian plates, the Great South and Canterbury basins were relatively tectonically stable, and not influenced by back-arc extension or Alpine deformation, following Late Cretaceous rifting. The Alpine Fault offset the basement terranes across Zealandia, such that those beneath the South Island are also present beneath parts of the North Island (e.g. Cassidy and Locke, 2010; Collanega et al., 2018; Cooper and Norris, 1994; Howell, 1980; Lamb et al., 2016; Muir et al., 2000; Tarling et al., 2019). In particular, the Dun Mountain-Maitai and Caples terranes, which underlie our study area, are present beneath the Auckland Volcanic Field in the North Island (Figure 1) (Cassidy and Locke, 2010; McGee et al., 2013; Spörli et al., 2015).

Late Cretaceous syn-rift strata within the Great South Basin, which were deposited unconformably onto the Permian-to-Triassic crystalline basement of the Caples and Dun Mountain-Maitai terranes, are dominated by siliciclastic rocks and coal measures of the Hoiho Group (Figure 1b) (Higgs et al., 2019; Killops et al., 1997; Sahoo et al., 2014). Widespread deposition of deep marine mudstones and siltstones occurred across the majority of the Great South and Canterbury Basins during the Cenozoic, with some carbonate deposition in the Oligocene-Miocene (Fig. 1b) (Bertoni et al., 2019; Chenrai and

157 Huuse, 2020; Morley et al., 2017). The Marshall Paraconformity forms the Oligocene-Eocene
158 boundary across the area and is purported to be related to the onset of the Antarctic circumpolar
159 current (Fulthorpe et al., 1996; Morley et al., 2017). Much of the shallow stratigraphy across the Great
160 South and Canterbury Basins has been reworked into contourite deposits (Figure 1b) (Fulthorpe et al.,
161 1996; Lu and Fulthorpe, 2004). At the present day, a series of steep-sided canyons traverse the seabed
162 across the area, often eroding down to the Marshall Paraconformity surface (Figure 1b).

163

164 2.2 Intraplate igneous activity across Zealandia

165 Following the breakup of Gondwana in the Late Cretaceous, widespread and long-lived magmatic and
166 volcanic activity has occurred in intraplate settings across Zealandia. Aside from back-arc rifting and
167 associated volcanism in the Taupo Volcanic Zone (1.5 Ma–Present), examples of Late Cretaceous
168 and/or Cenozoic intraplate volcanic systems include: the Auckland Volcanic Field (30 ka – 600 y BP)
169 on the North Island (Acocella et al., 2003; Cassidy and Locke, 2010; McGee et al., 2013); and the
170 Akaroa and Lyttleton volcanoes (12-6 Ma), and the Dunedin Volcano (16-11.7 Ma) of the Banks and
171 Otago Peninsulas, respectively, on the South Island (Figure 1) (Price and Chappell, 1975; Speight,
172 1943; Stipp and McDougall, 1968). Offshore New Zealand, the Auckland (~37–19, 25–12 Ma) and
173 Chatham islands (85–82, 41–35, 6–3 Ma) located towards the eastern and southern margins of
174 Zealandia, respectively, were also repeatedly active during the Late Cretaceous-to-Cenozoic (Adams,
175 1983; Grindley et al., 1977), with further magmatic and volcanic activity having been documented in
176 the Canterbury and Taranaki basins during the Miocene (Bischoff et al., 2017; Morley, 2018; Reeves
177 et al., 2018). A detailed catalogue of the timings of intraplate volcanism across Zealandia can be
178 found in Hoernle et al. (2006) and Timm et al. (2010), and references therein, with further examples
179 of intraplate volcanism shown in Figure 1a.

180 The causal mechanism for the diffuse Cenozoic-to-present record of intraplate volcanic activity across
181 Zealandia is difficult to reconcile with fixed hotspot- and rift-related processes (Timm et al., 2010).
182 For example, volcanic activity is not compatible with a plume-related origin as such a long record of

activity would require a static Zealandia relative to a 'fixed' mantle source; yet plate motion data indicate Zealandia has moved ~4000 km N/NW during the Cenozoic (Clouard and Bonneville, 2005; Hoernle et al., 2006; Sutherland, 1995; Wright et al., 2016). Furthermore, aside from igneous activity related to back-arc rifting in the Taupo Volcanic Zone, Cenozoic magmatism across Zealandia is not related to lithospheric thinning and extension, which ceased during the Late Cretaceous (Figure 1b) (Acocella et al., 2003; Kula et al., 2007; Laird and Bradshaw, 2004; Mortimer et al., 2019). The igneous rocks sampled onshore New Zealand also show an OIB-type affinity not compatible with rift-related magmatism; their composition, including silica-undersaturated nephelenites and basanites, suggests they were derived from an asthenospheric source with varying degrees of input from a metasomatised mantle lithosphere (Finn et al., 2005; Hoernle et al., 2006). Intraplate volcanism across Zealandia is instead proposed to relate to localised detachment of dense material from the base of the lithosphere, small-scale convection, and decompression melting of upwelling asthenosphere (Elkins-Tanton, 2005; Hoernle et al., 2006; Timm et al., 2009; Timm et al., 2010). As a driver for lithosphere detachment, it has been suggested that the lithosphere beneath Zealandia contains large amounts of garnet pyroxenites and eclogites following protracted subduction, creating a contrast between dense lower lithosphere and relatively less dense upper asthenosphere (Elkins-Tanton, 2005; Hoernle et al., 2006; Timm et al., 2009). Similarly, increased mantle water content in a post-subduction setting may decrease mantle viscosity and lower the peridotite solidus, resulting in small-scale convection at the base of the lithosphere (Elkins-Tanton, 2005; Kaislaniemi et al., 2014). A key component of this coupled lithosphere detachment and small-scale convection mechanism is that the magma source is not fixed in specific locations in the mantle or lithosphere, allowing individual intraplate volcanic systems to occur over widespread areas and long timescales.

3 Data and methods

3.1 Available data and seismic interpretation

In this study, we use 2D seismic reflection data from three different surveys (OMV, DUN and HUN), with a total line length of >50,000 km. These datasets were acquired over a range of years (1972,

2006, and 2008) and, accordingly, have different acquisition and processing parameters. Two of the surveys (OMV, DUN) record to ~8 s two-way travel-time (TWT), whilst the HUN survey records to ~5 s TWT. Seismic lines are typically oriented either NE-SW or NW-SE, and have a maximum spacing of 2 km in the NE direction and ~8 km in the NW direction (Figure 2). All seismic data are zero phase and displayed in normal polarity, such that a downward increase in acoustic impedance (e.g., the seabed) is represented by a peak (red) reflection, with a downward decrease in acoustic impedance represented by a trough (blue). The seabed across the study area is cut by multiple, steep-sided, up to ~0.5 s TWT deep canyons, which often produce geophysical artefacts (multiples) at deeper stratigraphic levels that partially obscure reflection configurations. There are no boreholes in the study area but we tie our seismic data to the Toroa-1 well, located ~140 km to the SW, to constrain ages of key stratigraphic units (Figure 1a). The magnetic data used in this study are shown as reduced to pole in order to place the anomalies vertically above the magnetic source (Figure 2).

3.2 Seismic resolution

The limit of separability (wavelength (λ)/4) within the sedimentary succession of interest, based on an average seismic velocity of ~3 km s^{-1} for the stratigraphic sequence derived from the Toroa-1 borehole (Figure 1) and an average dominant frequency of ~30 Hz, is ~25 m; the limit of visibility (λ/30), i.e. the thinnest structure that will be detected in the data, is ~3 m (Slatt, 2006). Features imaged in the seismic data that are thicker than the limit of separability will produce discrete reflections that can be linked to their top and base, whilst features with a thickness between the limits of separability and visibility will be displayed as tuned seismic reflection packages (Kallweit and Wood, 1982; Widess, 1973). Such tuned reflection packages occur because reflections from the top and base of the same feature interfere on their return to the surface and cannot be deconvolved (Brown, 2011).

No igneous features associated with the Tuatara Volcanic Field are penetrated by boreholes, so we do not know their composition or seismic velocity. However, based on comparison to the Maahunui Volcanic Field located in the northern Canterbury Basin, where the Resolution-1 boreholes intersects a gabbroic sill (Bischoff et al., 2020; Bischoff et al., 2019; Magee et al., 2019), and to volcanic fields

sampled onshore New Zealand (Hoernle et al., 2006; Németh and White, 2003; Timm et al., 2009), we infer the Tuatara Volcanic Field is likely dominantly mafic. From an average interval velocity of ~5.2 km s^{-1} for the gabbroic sill intersected by Resolution-1 (Magee et al., 2019), coupled with estimated velocity ranges for mafic volcanic fields imaged in seismic reflection data elsewhere (e.g., western India - ~3:3–5.5 km s^{-1}, Calvès et al. (2011); Australia, Bight Basin - ~2:4–6.7 km s^{-1}, Magee et al. (2013b); Australia, Bass Basin - 2:2–4.0 km s^{-1}, Reynolds et al. (2018)), we anticipate that igneous rocks within the Tuatara Volcanic Field likely have an average seismic velocity of 4.5±1.5 km s^{-1}. Combined with a dominant seismic frequency of ~30 Hz within the depth interval of the Tuatara Volcanic Field, our inferred velocities correspond to limits of separability and visibility of ~25–50 m and 3–7 m, respectively. As we do not know the detailed velocity structure of the volcanic province and surrounding strata, particularly its lateral variability, we do not depth-convert the seismic reflection data and present measurements in time rather than depth to avoid additional errors.

3.3 Interpreting and dating volcano-magmatic features

We identify and map a series of different igneous sills, lavas, and volcanoes across the study area based on their (e.g. Eide et al., 2018; Planke et al., 2005; Planke et al., 2000; Symonds et al., 1998; Thomson, 2005): (i) relatively high amplitude compared to stratigraphic reflections; (ii) positive polarity; (iii) limited lateral extent; and (iv) geometrical similarity to sills, lavas, and volcanoes observed elsewhere. Sills were also mapped based on whether their corresponding reflection cross-cuts, but does not offset background stratigraphic reflections (e.g. Magee et al., 2016; Planke et al., 2005; Thomson and Hutton, 2004). To constrain the relative age of inferred volcano-magmatic features, we mapped five stratigraphic horizons across the area that we correlated to the Tara-1 and Toroa-1 wells located ~130–140 km to the south (Figure 1 and Supplementary Figure 1): Top Coniacian (~86.3 Ma); Top Cretaceous (~66 Ma); Top Paleocene (~56 Ma); Top Early Eocene (~45.7 Ma); and the Marshall Paraconformity (Base Oligocene ~33.9 Ma). There is no well control on deeper stratigraphic levels throughout the Great South Basin, although a tentative top crystalline basement, corresponding to a high-amplitude reflection separating overlying continuous reflections from underlying chaotic reflectivity, is interpreted on individual sections (Sahoo et al., 2014; Uruski et al.,

2007; Uruski, 2010). From these mapped stratigraphic horizons, we can constrain the relative timing of emplacement of different igneous features by: (i) determining the age interval of strata that interpreted volcanoes and lavas were erupted onto (i.e. the syn-volcanic palaeosurface), and the age interval of strata that directly overlies and onlaps onto them (e.g. Magee et al., 2013b; Symonds et al., 1998); (ii) dating strata encasing sills, which the intrusions must post-date; and (iii) defining the age of strata onlapping onto intrusion-induced forced folds above sills, where observed, which formed at the contemporaneous free surface to accommodate sill intrusion (Hansen and Cartwright, 2006; Magee et al., 2017; Reeves et al., 2018; Trude et al., 2003).

As only 2D seismic reflection data are available, many volcano-magmatic features are only observed on individual 2D lines, meaning we cannot assess or quantify their individual 3D geometry. Where volcano-magmatic features can confidently be mapped across several 2D lines, we utilise the seismic software to interpolate our 2D horizon interpretations and recover their approximated 3D structure (see Hansen et al., 2008). Whilst this interpolation technique is broadly applied to extract information on the 3D geometry of volcanoes and sills imaged in 2D seismic reflection, the 2D seismic lines may not intersect the centre or maximum diameter of any specific feature (e.g., Hansen et al. 2008; Magee et al. 2013). Furthermore, we acknowledge that seemingly isolated features interpreted on different sections may in fact form part of a larger, singular structure. Quantitative measurements can therefore only be considered to represent minimum estimates. Finally, we note that some small volcano-magmatic features present in the study area may occur between and thus not be imaged by our 2D seismic grid.

4 Identification of volcano-magmatic structures in the Tuatara Volcanic Field

We recognise a variety of different intrusive and extrusive igneous features that we can differentiate based on their location relative a central structural high, which we term the ‘Central edifice’. For

clarity, here we sequentially describe and interpret the origin and age of: (i) high-amplitude reflectivity comprising the Central edifice; (ii) mound-like structures atop and beyond the lateral limits of the Central edifice; and (iii) intrusive features, and associated host rock structures, beyond the lateral limits of the main edifice.

4.1 Central edifice

4.1.1 Observations

The Tuatara Volcanic Field is characterised by a ~0.5 s TWT thick package of stacked, broadly sub-parallel, high-amplitude seismic reflectivity that forms a convex-upwards domal structure (Figures 2, 3, 4); we term this the Central edifice. The top of the reflection package has a positive polarity, indicating it corresponds to a downwards increase in acoustic impedance (e.g., Figs 3, 4). Beneath this high-amplitude reflection package, seismic reflections appear dimmer and more chaotic (i.e. they are 'washed out') compared to areas at the same structural level beyond the lateral limits of the Central edifice (Figs 3, 4). Despite the poorer imaging beneath the high-amplitude reflection package, we are able to tentatively map the underlying top acoustic basement and, occasionally, the Top Coniacian and Top Cretaceous horizons (Figs 3, 4); we note that the most prominent reflections often correspond to seafloor canyon-related multiples (Fig. 3). Some offset reflections across potential faults can also be tentatively identified on individual seismic sections (Figure 3).

In plan-view, the high-amplitude reflection package defining the Central edifice displays an elliptical geometry, covering ~270 km^2, with a NW-trending long axis 23 km in length and a 15 km long, NE-trending short axis (Figure 2b). The upper surface of the high-amplitude reflection package reaches 2 s TWT at its shallowest point in the centre and deepens to 2.5–3 s TWT around its margins (Figures 2b, 3, 4). At the deepest part of its upper surface, Upper Cretaceous strata onlap onto the high-amplitude reflection package (Figure 3), whilst at shallower depths it is onlapped and overlain by Early Eocene strata. In places, the top Paleocene horizon can be mapped through the upper portion of the high-amplitude reflection package (Figure 3, 4).

We also identify some areas of lower amplitude reflectivity within the reflection package, which typically correspond to mound-shaped features (see section 4.2), or reflections displaying a clinoform-like geometry (Figs 3, 4); i.e. they consist of gently dipping reflections with a sigmoidal geometry <100 ms TWT high. The top inflexion point of these sigmoidal reflections is typically horizontal across the reflection package (Figure 5).

4.1.2 Interpretation

We interpret the domal package of high-amplitude reflectivity as a series of stacked, tabular lava sequences based on: i) the high-amplitude and positive polarity of the reflections, consistent with a downwards increase in acoustic impedance from lower velocity (~3 km s^{-1}), lower density sedimentary rocks above into higher velocity (~4.5 km s^{-1}), higher density igneous lavas; ii) the inference that underlying reflections locally display a convex-upwards morphology, which could be a geophysical velocity 'pull-up' artefact akin to those observed beneath volcanoes elsewhere and related to seismic energy travelling through an overlying high velocity layer (e.g. Magee et al., 2013b; Sun et al., 2019a); iii) the lack of reflectivity beneath the package, as high impedance lavas can scatter and attenuate seismic energy, restricting imaging of underlying layers (e.g. Gallagher and Dromgoole, 2007; Maresh et al., 2006); and iv) the laterally discontinuous nature of the reflections, forming an isolated domal structure, suggestive of a non-sedimentary origin (Figure 3, 4). Similarities between the seismic expression of tabular lava sequences identified and confirmed by boreholes elsewhere and the domal high-amplitude reflection package we observed, supports our interpretation that the Central edifice comprises a stacked lava sequence (McLean et al., 2017; Quirie et al., 2019; Walker et al., 2019). Our tentative interpretation that normal faults can be recognised beneath the high-amplitude reflection package suggests that it may reside upon a horst-like structure; this inference remains contentious as we are unable to correlate interpreted faults across multiple seismic sections and thus cannot confirm the basement structure (Figure 3, 4).

Based on their location within and associated with the stacked lava sequences, we suggest the relatively low-amplitude, sigmoidal reflection packages may also be igneous in origin. In particular, we consider these sigmoidal reflection packages correspond to lava or hyaloclastite deltas, as they

appear similar in their geometry, structural setting, and seismic character to examples identified, and occasionally drilled, in other sedimentary basins (Planke et al., 2000; Wright et al., 2012). Using the sequence-stratigraphic terminology applied to clinoforms, the sigmoidal reflection packages described here represent dominantly progradational sequences, indicative of transport away from areas of higher relief, with little to no aggradation (Figure 5). The relatively small height (<100 ms TWT) and progradational character of these sequences suggests that they built outwards into a shallow water environment of similar depth to the clinoform height (~100-150 m) (Figure 1b) (Patruno and Helland-Hansen, 2018; Wright et al., 2012). The presence of potential lava and/or hyaloclastite deltas, coupled with its domal geometry, suggest the Central edifice of the Tuatara Volcanic Field may have formed a shallow-water bathymetric high during its formation (Figure 3).

At its deepest, the base of the Central edifice lava sequence occurs within Upper Cretaceous strata (i.e. extending just below the Top Coniacian), which also onlaps onto the lowermost section of the top lava sequence (Figure 3); these observations suggest lava extrusion to form the Central edifice initiated in the Upper Cretaceous, perhaps towards the end of the Coniacian (~86 Ma). It is difficult to determine whether the edifice was constructed during a single event or through multiple, periodic extrusive phases because we cannot distinguish whether the onlapping Palaeocene and Early Eocene strata was deposited around a pre-existing dome or on a progressively growing structure. However, on some 2D seismic lines, interpreted stratigraphic horizons can seemingly be mapped into the stacked lavas sequences, and thus potentially represent syn-volcanic paleosurfaces that allow us to constrain edifice growth (Figure 3, 4). The interpreted top basement horizon continues beneath and thus predates the formation of the Central edifice (Figure 4). Whilst the top Coniacian horizon also appears to mostly continue beneath the Central edifice (Figure 4), in some areas it extends into the highly reflective lava sequences, suggesting that this interval corresponds to an early stage of Central edifice construction (Figure 3). At shallow depths, the top Early Eocene horizon blankets the edifice indicating that it postdates its formation. Between these maximum and minimum age constraints, the top Paleocene horizon appears to represent the basal surface of a lava sequence in the upper parts of

the high-amplitude reflection package (Figure 4), suggesting the Central edifice formed through at least two extrusive events in the Upper Cretaceous and towards the end Palaeocene.

4.2 Mound shaped features

4.2.1 Observations

We identify a total of 69 mound-shaped features distributed atop, within, and around the Central edifice at multiple stratigraphic levels spanning the Cretaceous to Early Eocene (Figure 2b, 6). These mound-shaped features are characterised by a variable amplitude, typically positive polarity top surface and a sub-horizontal, conformable basal reflection (Fig. 6). Where reflections are resolved within the mounds, they are typically low- to moderate-amplitude and either parallel the top mound surface or appear sub-horizontal (Figure 5b). The majority of mounds have a prominent peak (Figure 6b, e, f), although some display a flatter top (Figure 6a, c). The mounds typically have minimum heights of ~25 ms TWT and basal diameters of ~1–2 km, with the largest reaching minimum heights of up to 400 ms TWT and basal diameters of ~3 km (Figure 6).

The mounds are located proximal to the Central edifice, with the majority (~43) situated atop or within the high amplitude reflection package (Figure 3, 4, 7a). The top of the edifice is characterised by two large conical features surrounded by stacked lava sequences (Figure 2b, 6a). Further mounds are identified at different stratigraphic levels within the edifice itself (Figure 3, 6a). In some instances we observe that the high-amplitude reflections interpreted as lavas are often spatially related to the mounds identified here, being located around their margins and often draping atop the structures (Figure 6a, e).

Reflections above the mounds locally appear to deflect upwards, forming anticlinal folds, which occasionally host crestal faults (Figure 6a, d). Within one of these supra-mound folds, a bright, high-amplitude, and horizontal reflection cross-cuts the folded strata (Figure 6e). In some instances, the mounds are associated with underlying vertical zones of seismic disturbance characterised relatively low-amplitudes and reflection deflection (e.g., Figure 6f).

To the south of the Central edifice, we identify multiple high-amplitude, positive polarity, tuned reflection packages within the Lower Eocene succession (Figure 2a, 4, 8). These high-amplitude reflections are situated beneath, but close to, the top Early Eocene horizon and are downlapped by Early Eocene-aged strata (Figure 2, 8). In places, the high-amplitude reflections appear to cross-cut and/or truncate underlying reflections (Figure 8). The amplitude of these high-amplitude reflections decreases towards a small (~300 m wide), 60 ms TWT high mound is developed (Figure 8). This central mound is underlain by a zone of chaotic and upturned stratal reflections extending downwards from ~2.4–2.7 s TWT, before transitioning into a wide (from ~1 to ~2 km) acoustically transparent zone >2.7 s TWT (Figure 8). A ~0.1 s TWT deep depression is located above the mound at the Marshall Paraconformity surface (Figure 8).

4.2.2 Interpretation

Based on the following lines of evidence we interpret that the mound-shaped features are buried volcanoes: i) the relative location of the mounds within the stacked lava sequences and surrounding the Central edifice (Figure 7a), with the volcanoes likely responsible for the eruption of the lavas (Reynolds et al., 2017); ii) the mound-shaped geometry of the structures atop a conformable base and likely conical morphology of the structures in plan-view, resembling typical volcano geometries observed in seismic reflection data (Morley, 2018) (Figure 2b; 8); iii) the positive amplitude seismic character of the mounds, consistent with a positive impedance contrast expected between igneous volcanic rocks and overlying sedimentary material; and iv) where internal structures are resolved within the mounds, reflections parallel the top surface, consistent with volcano construction via the proportional addition of material to their summit and flanks (e.g., Magee et al., 2013). The occurrence of flat tops on some volcanoes may be indicative of later erosion as they emerge at the paleo-seasurface (Bischoff et al., 2019; Bischoff et al., 2017), or may simply be a product of the volcano being intersected along its flank (not across its centre) by the 2D seismic lines. Sub-horizontal reflections within volcanoes may also correspond to the cut-effect of the seismic line sampling the flank of the structure. Although we are unable to determine the eruptive history of individual volcanoes, the distribution of multiple, relatively small volcanoes within a relatively localised area

(typically 20-30 km from the centre of the Central edifice), suggests that they may represent a monogenetic volcanic field (Németh, 2010; Németh and White, 2003). Geometrically, the distribution of volcanoes bears similarities to that of the monogenetic Auckland Volcanic Field in the North Island (Cassidy and Locke, 2010; Rout et al., 1993; Spörli and Eastwood, 1997), as well as monogenetic volcanic fields identified in seismic reflection data elsewhere (Bischoff et al., 2020; Bischoff et al., 2019; McLean et al., 2017).

Due to their clustering within and surrounding the Central edifice, we suggest that, at least for the upper parts of the domal edifice, the volcanoes may have been responsible for the eruption of the stacked lava packages, with the majority of activity occurring in the Paleocene. The volcanoes are located at different stratigraphic levels within the reflection package, with buried cones likely responsible for the eruption of older lavas (Figure 3, 6a). Additional volcanoes, and potential fissure vents, may be present at greater depths beneath the edifice although we are unable to resolve these structures due to a lack of imaging beneath the thick lava sequence (Quirie et al., 2019) (Figure 3).

Cumulatively the rocks comprising volcanoes (e.g., crystalline lavas, volcaniclastics) typically have a lower porosity than encasing and overlying, initially unconsolidated sedimentary material (e.g. Chopra and Marfurt, 2012). Upon burial, volcanoes therefore commonly compact less than the surrounding strata, promoting a differential compaction that results in the formation of anticlinal folds and associated outer-arc extension crestal faults above the volcano (e.g. Sun et al., 2019b; Zhao et al., 2014), similar to those we describe here (Figure 6a, c, d). Buried volcanoes have been shown to act as conduits for later fluid flow in the subsurface (Holford et al., 2017; Sun et al., 2019b). We interpret the sub-horizontal, high-amplitude reflection within the overlying differential compaction fold of one volcano as a ‘flat-spot’, likely corresponding to a trapped gas pocket (Figure 6e).

To the south of the Central edifice, we interpret the small mound as a small volcano, with the adjacent high amplitude reflections interpreted as associated lava flows (Figure 8). This interpretation is corroborated by zone of chaotic and washed out reflectivity beneath the structure and the immediately adjacent upturned strata (Figure 8). The upturned strata are interpreted as a velocity pull-up, a seismic artefact generated due to relatively high velocities beneath the structure, suggestive of igneous

material. The sub-vertical chaotic reflectivity beneath the volcano may correspond to igneous dykes or pipes, forming a vertical plumbing system to individual volcanoes (Figure 6f, 8) (Wall et al., 2010). The apparent small size of this cone may be a result of the seismic section only intersecting the margin of the structure, rather than passing through its centre (Figure 8). The volcano is associated with a series of Early Eocene high-amplitude reflections, which we interpret as erupted lava flows (Figure 8). The brightening of the lava flows away from the volcanic cone likely represents a decrease in thickness, and an associated increase in seismic tuning, towards their termination (Kallweit and Wood, 1982; Smallwood and Maresh, 2002; Widess, 1973) (Figure 8). The truncation of underlying strata by the lava flows may correspond to the formation of lava channels and the associated bulldozing and erosion of the underlying stratigraphy (Sun et al., 2019a). The onlapping of Early Eocene strata onto the lava flow may relate to the dominantly contouritic nature of the stratigraphy in this interval (Figure 1b). The depression on the Marshall Paraconformity surface co-located above the volcanic cone appears to have formed due to fluid expulsion following burial, with the volcano focussing migrating fluids (Figure 8) (Holford et al., 2017; Sun et al., 2019b).

4.3 High-amplitude transgressive reflections

4.3.1 Observations

Aside from the high-amplitude, sub-horizontal reflection packages interpreted as lava flows, we identify 92 high-amplitude, positive polarity reflections that are laterally discontinuous and commonly display transgressive, saucer-shaped or inclined morphologies (Figure 9). These features typically have lengths ranging from 1-3 km, individually span depth ranges up to ~0.2 s TWT, and are observed at different stratigraphic levels between the pre-Coniacian and the Paleocene (Figure 7b, 9). Many of these transgressive high-amplitude reflections are located beneath interpreted volcanoes, although some appear independent of extrusive features and occur up to 30-40 km from the Central edifice (Figure 7b). The majority of these high-amplitude transgressive reflections are associated with clear anticlinal folds in the overlying strata, the outer inflection points of which directly overlie the lateral terminations of the high-amplitude reflection (Figure 9). These folds can be identified

476 throughout Late Cretaceous-to-Early Eocene strata, with strata onlapping onto their margins (Figure
477 9).

478 ***4.3.2 Interpretation***

479 We interpret these high-amplitude, transgressive reflections as igneous sills because: i) the high
480 amplitude and positive reflection that defines their upper surface is consistent with an acoustically
481 hard lithology, such as igneous material (Hansen et al., 2008); ii) they transgress and cross-cut
482 background reflections, distinguishing these feature from the aforementioned lava flows, but do not
483 offset strata and thus are not faults; and iii) their typical saucer-shaped geometry is similar to sheet
484 intrusions identified onshore (Galerne et al., 2011; Ledevin et al., 2012; Polteau et al., 2008) and
485 igneous sills resolved in seismic data, some of which have been drilled, from the Rockall Basin
486 (Morewood et al., 2004; Thomson and Hutton, 2004), Faroe-Shetland Basin (McLean et al., 2017;
487 Smallwood and Maresh, 2002), offshore Australia (Jackson, 2012; Magee et al., 2017; Magee et al.,
488 2016), and in the Canterbury Basin offshore New Zealand (Bischoff et al., 2017; Reeves et al., 2018).
489 We are able to relate the 92 high-amplitude features identified here as corresponding to ~79 individual
490 sills, with some sills resolved across multiple seismic sections. Additional sills may be present
491 beneath the main central dome, but they are not resolved in our data (Figure 3, 4, 7b). Overall, we
492 classify the mapped intrusions as a sill-complex (Magee et al. 2016).
493
494 We interpret the folds overlying the sills as intrusion-induced forced folds that formed via overburden
495 uplift to accommodate shallow-level magma emplacement (Hansen and Cartwright, 2006; Magee et
496 al., 2013a; Reeves et al., 2018; Trude et al., 2003). Recognition of overlying strata onlapping onto
497 these folds indicates the top fold surface corresponded to the syn-emplacement palaeosurface (Figure
498 9), and can be used to date intrusion (e.g. Trude et al., 2003). For those sills not overlain by forced
499 folds we use the age of the encasing strata as a maximum estimate for emplacement timing. From
500 these seismic-stratigraphic onlap relationships we estimate sills ages within the Tuatara Volcanic
501 Field range from the pre-Santonian (Top Teratan - >86.3 Ma) to Early Eocene (Top Heretaungan –
502 45.7 Ma), representing over 40 Myr of magmatic activity.

5 Distribution and age of volcano-magmatic structures in the Tuatara Volcanic Field

The Central edifice of the Tuatara Volcanic Field, which comprises stacked lava sequences, hyaloclastites, and volcanoes covers a ~270 km^2 elliptical area that is elongated in a NW-SE orientation (Figure 2). Igneous sills are much more widely distributed around the edifice than the volcanoes (Figure 7b). A subtle WNW-ESE trend is present in the spatial distribution of volcanoes and sills; this is more pronounced with the volcanoes (Figure 7). By determining the age of emplacement for the sills and volcanic cones, we assign these structures to stratigraphic intervals and examine how their distribution evolved temporally. Those volcanoes and sills emplaced prior to the Santonian (>86.3 Ma) are typically located ~30 km to the southeast of the Central edifice, with some pre-Santonian aged sills also present northeast of the Central edifice (Figure 7). Late Cretaceous sills (from 86.3-66 Ma) are located closer to the central dome (~20 km) but distributed around its SW, SE, and NE sides (Figure 7b). No Late Cretaceous volcanoes were identified. Paleocene-aged structures are the most abundant across the area. Paleocene-aged volcanoes are relatively tightly clustered around the central dome compared to older volcanoes (~10 km) (Figure 7a). Paleocene sills are more proximal to the Central edifice relative to older sills, although they are still relatively distributed compared to volcanoes of the same age (Figure 7b). A cluster of Paleocene sills occur immediately west-northwest of the central dome. Early Eocene and younger sills and volcanoes occur to the northwest of the main edifice, with the exception of one sill straddling the Paleocene-Eocene boundary (Figure 9d), suggesting a broad north-westward migration of igneous activity from the pre-Santonian to the Early Eocene (Figure 7). The youngest structures, an Early Eocene sill (56-45.7 Ma) and a volcanoes younger than the Early Eocene (<45.7 Ma) (Figure 6b), are both located ~25-30 km to the northwest of the Central edifice, whereas the oldest interpreted structures are located approximately ~35 km to the southeast (Figure 7).

Given the mapped volcanoes and sills display a similar spatial and temporal distribution (Figure 7), with some intrusions seemingly extending up to the base of some volcanic edifices (e.g., Figure 6c), we consider magma was primarily delivered to the surface via the sill-complex. Importantly, recognising the mapped sill-complex likely fed the Tuatara Volcanic Field implies individual volcanoes were connected (Magee et al., 2016); i.e. activity at one volcano could have been linked to eruption at another as they probably shared a plumbing system. We also note that some volcanoes are underlain by pronounced vertical seismic disturbances, which we interpret as corresponding to dykes (Figure 6f, 7) (Magee and Jackson; Magee and Jackson, 2020; Wall et al., 2010). These dykes appear to feed isolated volcanic cones away from the central edifice (Figure 7a).

6 Discussion

The Tuatara Volcanic Field occupies a relatively localised (~270 km^2) setting above the Livingstone Fault, which marks the boundary between the Dun Mountain-Maitai Terrane to the south, and the Caples Terrane in the north (Figure 10) (Mortimer et al., 2002; Tarling et al., 2019). Here, we examine the controls on the localisation, geometry, and longevity of intraplate volcanic activity at the Tuatara Volcanic Field. We also discuss how our observations of the internal structure and plumbing system of the Tuatara Volcanic Field may relate to the Auckland Volcanic Field and enhance our understanding of intraplate volcanic systems generally.

6.1 Controls on the location of the Tuatara Volcanic Field

Intraplate volcanism appears to display a relatively random distribution across Zealandia (Hoernle et al., 2006; Timm et al., 2010); similar areas of diffuse intraplate volcanism have been identified across the Turkish-Iranian Plateau (Kaislaniemi et al., 2014). Such diffuse regions of intraplate volcanism have been related to decompression melting of upwelling asthenosphere into areas where Rayleigh-Taylor instabilities and/or small-scale mantle convection, which occur due to density contrasts at the lithosphere-asthenosphere boundary and/or hydrated mantle following protracted subduction, has detached lithospheric material (Elkins-Tanton, 2005; Hoernle et al., 2006; Kaislaniemi et al., 2014). According to these models, intraplate volcanic systems are located directly above the seemingly

554 randomly distributed areas of detaching lithosphere and associated decompression melting (Elkins-
555 Tanton, 2005; Hoernle et al., 2006; Kaislaniemi et al., 2014). However, because some volcanic
556 systems, such as those on the Chatham Islands and Banks Peninsula, display repeated phases of
557 activity with long intervening periods (Figure 1) (Hoernle et al., 2006; Timm et al., 2009), it is
558 necessary to consider how localised areas of lithospheric detachment and volcanic activity could be
559 rejuvenated.

560 We consider lithospheric detachment as the likely mechanism for activity at the Tuatara Volcanic
561 Field, which we suggest is reflected in its elliptical geometry, similar to that of the Auckland Volcanic
562 Field (Spörli and Eastwood, 1997); i.e. the areal extent of the Tuatara Volcanic Field likely marks the
563 limits of an underlying zone of melt where the lithosphere detached. However, we also note that the
564 Tuatara Volcanic Field overlies the Livingstone Fault, which marks the boundary between the Caples
565 and Dun Matai terranes. The Auckland Volcanic Field and volcanoes on the Banks Peninsula are also
566 co-located along prominent basement terrane boundaries, namely the same boundary as the Tuatara
567 Volcanic Field, between the Dun Mountain-Maitai and Caples terranes, and the Rakaia and Pahau
568 terranes respectively (Figure 1a) (Eccles et al., 2005; Mortimer et al., 2002; Tarling et al., 2019). This
569 co-location of volcanic fields with major basement terrane boundaries questions whether the
570 localisation of intraplate volcanic systems may, at least partially, be controlled by pre-existing
571 structures. For example, faults have been shown to act as conduits for magma and may thus spatially
572 correlate with the plumbing systems of volcanoes (e.g. Mazzarini, 2007). Based on the overall
573 location of the Tuatara Volcanic Field and the approximate NW-alignment of constituent volcanoes
574 and sills, parallel to the underlying basement terranes and Livingstone Fault (Figure 2b), we suggest
575 that the location of the Tuatara Volcanic Field was primarily controlled by underlying pre-existing
576 structures. In particular, we envisage that the Livingstone Fault, and perhaps sub-vertical foliations
577 within the Dun Mountain-Matai terrane (Eccles et al., 2005), provided viable pathways for magma
578 ascending through the crust.

579 Considering the location of the Tuatara Volcanic Field is linked to that of the Livingstone Fault at
580 upper crustal depths, we in turn question whether the site of lithosphere detachment could have been

581 influenced by pre-existing structures. Regional seismic reflection data located offshore of the South
582 Island indicate that the Livingstone Fault extends down to at least the Moho (Figure 1, 10c) (Mortimer
583 et al., 2002). If the Dun Mountain-Matai and Caples terranes, which accreted to the southern margin
584 of Gondwana, are characterised by different lithospheric thicknesses and properties, we suggest that
585 the Livingstone Fault could extend deeper and have some expression at the base of the lithosphere
586 (i.e. a change in lithospheric thickness or narrow keel; Figure 10c) (Eccles et al., 2005; Tarling et al.,
587 2019). Such promontories at the base of the lithosphere may provide a first-order control on the
588 development of small-scale mantle convection cells and Rayleigh-Taylor instabilities, focussing the
589 detachment of lithospheric material (Figure 10c). Elsewhere, small-scale convection cells will be
590 controlled by the spacing between adjacent cells, causing lithosphere detachment and the associated
591 intraplate volcanic systems to not be 'directly' related to a pre-existing structure and appear randomly
592 distributed (Kaislaniemi et al., 2014). Therefore, whilst pre-existing structures appear to control, or at
593 least influence, the location of some individual intraplate volcanic systems (e.g., the Tuatara Volcanic
594 Field), it also allows for a random background distribution of intraplate volcanic systems that bear no
595 apparent relation to pre-existing structure.

596 Although spatial correlation suggests the location of the Tuatara Volcanic Field as a whole was
597 influenced by pre-existing structures, it is difficult to ascertain whether its individual intrusive or
598 extrusive components were similarly structurally controlled. For example, at shallow depths within
599 the Tuatara Volcanic Field, we are unable to fully constrain the geometry of rift-related faults beneath
600 the Central edifice, although faults typically strike NE-SW across the Great South and Canterbury
601 Basins (Phillips and McCaffrey, 2019; Uruski et al., 2007; Uruski, 2010). Overall, we suggest the
602 transition from vertical magma ascent from the base of the lithosphere, likely via dykes, to formation
603 of a sill-complex within the Great South Basin was related to a local change in the differential stress
604 field at shallower depths (Stephens et al., 2017), and/or deflection of magma pathways along sub-
605 horizontal boundaries (Kavanagh et al., 2006; Kenny et al., 2012).

606 ## 6.2 Controls on the longevity of the Tuatara Volcanic Field

607 The longevity of intraplate volcanic systems across Zealandia (i.e. those not related to rift activity) is
608 proposed to be determined by the time taken for the area of material detached from the base of the
609 lithosphere to anneal, thereby stopping any decompression melting of upwelling asthenosphere
610 (Timm et al., 2009). Accordingly, the larger the diameter and depth of the volume of detached
611 lithosphere, the greater the expected magmatism, either in magnitude or longevity. The magnitude of
612 melting in turn influences the resultant style of volcanism; low-Si monogenetic volcanic fields are
613 thought to relate to small areas of detaching lithosphere producing small-degree melts with larger
614 shield volcanoes (i.e. those at Banks Peninsula) associated with larger and deeper areas of detaching
615 lithosphere producing larger-degrees of melting (Hoernle et al., 2006).

616 We document a ~40 Myr record of magmatic and volcanic activity across the Tuatara Volcanic Field
617 lasting from ~85–45 Ma. Earlier volcano-magmatic features may be present at deeper levels, although
618 we are unable to resolve structures at these depths (Figure 3, 4). The earliest phases of activity in the
619 Tuatara Volcanic Field appear to post-date the cessation of subduction along the southern margin of
620 Gondwana caused by impingement of the Hikurangi Plateau (Davy et al., 2008), and overlap with
621 rifting associated with Gondwana breakup, which lasted until ~80 Ma (Kula et al., 2007; Tulloch et
622 al., 2019). The vast majority of volcano-magmatic activity in the Tuatara Volcanic Field and across
623 Zealandia occurred in an intraplate setting, with the main period of activity during the Paleocene
624 (Figure 10a).

625 The ages of sills and volcanoes identified in the Tuatara Volcanic Field migrates towards the
626 northwest through time, following the orientation of the underlying basement terranes (Figure 7).
627 Similarly, at the Banks Peninsula, volcanic activity initially occurs at the Lyttelton Volcano in the
628 northwest (12.3-10.4 Ma), before migrating to the Akaroa Volcano ~25 km southeast (9.4-6.8 Ma),
629 correlating to the NW-trending terrane boundary between the Pahau and Rakaia terranes, albeit
630 migrating in the opposite direction to that observed at the Tuatara Volcanic Field (Timm et al., 2009).
631 In the case of Banks Peninsula, this may reflect progressive lithosphere detachment towards the
632 southeast along the terrane boundary; as the lithosphere begins to anneal beneath the Lyttelton
633 Volcano, further detachment occurs to the southeast leading to activity at the Akaroa Volcano (Timm

et al., 2009). We propose a similar mechanism of along-strike progressive lithospheric detachment focused along the expression of the Livingstone Fault at the lithosphere-asthenosphere boundary to explain the longevity and age progression within the Tuatara Volcanic Field (Figure 11) (Mortimer, 2004). In particular, we suggest such localisation by pre-existing structures may result in a quasi-periodic 'dripping' of material from the base of the lithosphere, focussing magmatic upwelling and inhibiting the complete annealing of the lithosphere over prolonged (>10 Myr) periods. That monogenetic volcanic fields are typically characterised by small-degree melts (Hoernle et al., 2006; Timm et al., 2009) suggests this quasi-periodic dripping is characterised by relatively small, but relatively frequent detaching of lithospheric material.

6.3 Implications for intraplate volcanism

We document the 3D geometry and longevity of an intraplate volcanic system, highlighting that seismic reflection data can potentially provide important insights into the processes driving intraplate volcanism. For example, the recently active (last eruption 600y before present) Auckland Volcanic Field is situated in the same structural setting, i.e. above the terrane boundary between the Dun-Mountain-Maitai and Caples terranes represented by the Livingstone Fault, as the Tuatara Volcanic Field on the opposite side of the Alpine Fault on the North Island (Figure 10b) (e.g. Cassidy and Locke, 2010; Lindsay et al., 2011; McGee et al., 2013; Rout et al., 1993; Spörli et al., 2015; Tarling et al., 2019). Both volcanic fields display similar geometric characteristics at the surface: the Auckland Volcanic Field is characterised by ~50 individual volcanic centres (each typically ~1–2 km in diameter) distributed across a roughly elliptical area with a ~29 km long axis and a short axis of ~16 km (~375 km^2) (Lindsay et al., 2011; Spörli and Eastwood, 1997); this is compared to 69 volcanoes (typically 1–2 km in diameter) identified within the 23 km x 15 km (~270 km^2) Tuatara Volcanic Field. The Tuatara Volcanic Field may thus represent a crucial ancient analogue to the Auckland Volcanic Field, potentially helping to constrain our understanding of the currently uncertain magma plumbing system and subsurface geology of the latter. In particular, the shallow-level plumbing system of the Tuatara Volcanic Field appears dominated by interconnected sills, with only isolated dykes interpreted distally with respect to the Central edifice (Figure 6f). If the Auckland Volcanic

Field also comprises a shallow-level, sill-dominated plumbing system, it is plausible that individual sills are linked such that (Magee et al., 2016): (i) activity at one could instigate activity at another; and/or (ii) pre-eruption warning signals (e.g., ground deformation and seismicity) may be laterally offset from the subsequent eruption site. Our work also implies that extinct volcanoes may be buried beneath the current exposure of the Auckland Volcanic Field; these buried volcanoes could provide pathways for fluid/gas escape (e.g., Figure 6b) (e.g., Holford et al., 2017; Sun et al., 2019b). Finally, whilst we are unable to directly comment on the likely longevity of volcanic activity in the Auckland Volcanic Field, observations from the Tuatara Field described here suggest that volcanic fields partly controlled by pre-existing structures could periodically be rejuvenated. Overall, hazard assessment of the Auckland Volcanic Field should take into account potential constraints on the location, geometry, and longevity of the system afforded by our study of the analogue Tuatara Volcanic Field.

7 Conclusions

We use seismic reflection data to image and document a newly discovered volcanic field, which we name the Tuatara Volcanic Field, located in the Great South Basin, offshore of the South Island of New Zealand. The ~270 km^2 Tuatara Volcanic Field is characterised by a central edifice comprising stacked lava and hyaloclastite sequences surrounded by 69 volcanoes connected by a sill-complex. Igneous activity occurred periodically over 40 Myr, beginning after rifting in the Late Cretaceous (~85 Ma) and continuing until the Early-to-Mid Eocene (~45 Ma). The Tuatara Volcanic Field thus represents one of the longest-lived volcanic systems in Zealandia and potentially elsewhere. The location of the Tuatara Volcanic Field coincides with the Livingstone Fault, a crustal-to-lithosphere scale boundary between the Dun Mountain-Maitai and Caples terranes, which we suggest facilitated magma ascent. Activity within the field migrates towards the northwest and to higher stratigraphic levels through time, following the orientation of the underlying basement structure. We suggest that the Livingstone Fault had some expression at the base of the lithosphere, which periodically promoted detachment of material from the lithosphere by Rayleigh-Taylor instabilities and/or small-scale

687 mantle convection. Decompression melting of upwelling asthenosphere into this area of detached
688 lithosphere likely controlled the site of the Tuatara Volcanic Field. Where such pre-existing structures
689 are absent, lithosphere detachment and intraplate volcanism may occur randomly and display shorter
690 periods of activity.

691 The geometry and structural setting of the Tuatara Volcanic Field resembles the Auckland Volcanic
692 Field; the locations of both volcanic fields appear to be controlled by the pre-existing Livingstone
693 Fault and terrane boundary. We suggest that the Tuatara Volcanic Field represents an ancient
694 analogue to the Auckland Volcanic Field. Our observations of the internal structure and longevity of
695 the Tuatara Volcanic Field may thus provide important insight into potential future activity at the
696 Auckland Volcanic Field. In particular, whilst magma transport is dominantly vertical throughout the
697 lithosphere, the plumbing system of the Auckland Volcanic Field may be characterised by a sill-
698 complex that connects and controls the distribution of volcanoes within the field. Furthermore, we
699 postulate that the longevity and progression of activity at the Tuatara Volcanic Field could imply that
700 the Auckland Volcanic Field is perhaps relatively early in its evolution and that activity may migrate
701 along the pre-existing structure across geological time. In this study, we have characterised the
702 internal plumbing system of a newly-discovered volcanic system offshore New Zealand. We highlight
703 how pre-existing crustal and lithospheric structure exert an important influence over the location and
704 longevity of individual intraplate volcanic systems. We offer insights into the internal structure and
705 plumbing system of these volcanic fields that may be applicable to other ancient and active intraplate
706 systems.

707

708

709 # Figure Captions

710

711 Figure 1 – A) Onshore relief and offshore bathymetry map of the South Island of New Zealand
712 highlighting the location of the Tuatara Volcanic Field and selected further intraplate volcanic
713 products across the South Island. Also shown are the locations of the major terrane boundaries across

714 the area (after Mortimer et al 2002). Inset – Map showing the regional basement geology across New
715 Zealand. B) Tectono-stratigraphic column showing the major stratigraphy present in the Great South
716 Basin, as well as the timings of regional tectonics and volcanism. After Bertoni et al. (2019); Higgs et
717 al. (2019); Mortimer et al. (2014).

718 Figure 2 – A) Magnetic anomaly map across the northern part of the Great South Basin. Data are
719 reduced to pole in order to place the anomalies vertically above the magnetic source. The locations of
720 major magnetic anomalies are shown after Tulloch et al. (2019) and Sutherland et al. (1999). The
721 magnetic data are courtesy of the NZ SEEBASE database (Pryer et al., 2013). B) Two-way-time
722 structure map of the top surface of the central edifice of the Tuatara Volcanic Field. The locations of
723 prominent volcanic cones are shown by the white triangles. See Figure 1 for location.

724 Figure 3 – Uninterpreted and interpreted NW-SE oriented seismic section across the Tuatata Volcanic
725 Field. The central edifice of the field is identified as a package of high-amplitude reflectivity, with
726 igneous sills and volcanic cones identified around the main structure. Image quality is greatly reduced
727 beneath the main edifice. See Figure 2 for location.

728 Figure 4 – Uninterpreted and interpreted NE-SW oriented seismic section across the Tuatara Volcanic
729 Field. The central edifice (shown in grey) is surrounded by multiple volcanic cones and igneous sills.
730 Image quality is greatly reduced beneath the central edifice. See Figure 2 for location.

731 Figure 5 – Close-up seismic sections and interpretations of the tabular lava sequences that comprise
732 the central edifice of the Tuatara Volcanic Field. Stacked lava sequences, individual volcanic cones
733 and lava delta sequences are highlighted in the interpretations. See Figure 2 for location.

734 Figure 6 – Interpreted seismic sections highlighting the morphology and seismic expression of
735 volcanic cones within the Tuatara Volcanic Field. See Figure 7 for the locations of individual
736 sections.

737 Figure 7 – A) Map showing the age and distribution of interpreted volcanic cones surrounding the
738 Tuatara Volcanic Field. B) Map showing the age of emplacement and distribution of igneous sills

739 within and surrounding the Tuatara Volcanic Field. Note that the igneous sills are more widely
740 distributed around the central edifice compared to the volcanic cones.

741 Figure 8 – Uninterpreted and interpreted seismic section showing a minor volcanic cone to the south
742 of the main edifice. See Figure 2 for location. Note the presence of Early Eocene aged lava flows
743 associated with the volcanic cone.

744 Figure 9 – Interpreted seismic sections showing a number of different sills interpreted throughout the
745 area. See Figure 7 for location. The age of sill emplacement can be estimated as the age of the strata
746 onlapping onto the identified forced folds.

747 Figure 10 – A) Schematic cartoon showing the overall evolution of the Tuatara Volcanic Field. Sill
748 emplacement and volcanism begins in the Late Cretaceous, with the majority of activity, including the
749 formation of the majority of the central edifice occurring in the Paleocene. Activity migrates towards
750 the northwest and wanes throughout the early Eocene, before the Tuatara Field becomes buried. B)
751 Map showing the distribution of sills and volcanic cones within the Tuatara Volcanic Field. The
752 distribution of volcano-magmatic features is co-located with the Livingstone Fault, forming the
753 boundary between the Caples and Dun Mountain-Maitai Terranes. Inset – Cartoon showing the setting
754 of the Auckland Volcanic Field, located between the same basement terranes on the North Island of
755 New Zealand. C) Regional model for the localisation of activity in the Tuatara Volcanic Field. Upper
756 crustal basement terranes are based on the SESI seismic section along the east coast of the South
757 Island of New, after Mortimer et al. (2002). The lower part of the figure shows the hypothesised
758 model for lithosphere detachment and melt generation in the lithosphere. See Figure 1 for location of
759 SESI seismic section.

760 Figure 11 – 3D block model showing the geometry of the Tuatara Volcanic Field and its hypothesised
761 link to magma generation at the base of the lithosphere. Areas of detaching material from the base of
762 the lithosphere promote decompression melting of upwelling asthenosphere. The detachment of
763 lithospheric material progressively migrates northwest-wards along the Livingstone Fault terrane
764 boundary, causing the age progression identified in the Tuatara Volcanic Field. The field is thought to

765 be dominated by vertical magma transport throughout the lithosphere, and is dominated by sills in the
766 upper crust.

767 Supplementary Figure 1 – Interpreted seismic section linking the study area to the nearby Toroa-1
768 borehole, providing age constraints on the shallow sedimentary succession of the Tuatara Volcanic
769 Field. Although located a great distance from the study area, the intervening geology between the
770 borehole and the Tuatara Volcanic Field is relatively simple, dominated by post-rift strata allowing us
771 to correlate horizons across the study area. See Figure 2 for location.

772

773 References

774 Acocella, V., Spinks, K., Cole, J., Nicol, A., 2003. Oblique back arc rifting of Taupo
775 Volcanic Zone, New Zealand. Tectonics 22.

776 Adams, C.J., 1983. Age of the volcanoes and granite basement of the Auckland Islands,
777 Southwest Pacific. New Zealand Journal of Geology and Geophysics 26, 227-237.

778 Adams, R.D., 1962. Thickness of the earth's crust beneath the Campbell Plateau. New
779 Zealand Journal of Geology and Geophysics 5, 74-85.

780 Beggs, J., 1993. Depositional and tectonic history of the Great South Basin. South Pacific
781 sedimentary basins. Sedimentary basins of the World 2, 365-373.

782 Bertoni, C., Gan, Y., Paganoni, M., Mayer, J., Cartwright, J., Martin, J., Van Rensbergen, P.,
783 Wunderlich, A., Clare, A., 2019. Late Paleocene pipe swarm in the Great South – Canterbury
784 Basin (New Zealand). Marine and Petroleum Geology 107, 451-466.

785 Bischoff, A., Nicol, A., Barrier, A., Wang, H., 2020. Characterization of a Middle Miocene
786 Monogenetic Volcanic Field Buried in the Canterbury Basin, New Zealand – Part II.

787 Bischoff, A., Nicol, A., Rossetti, M., Kennedy, B., 2019. Characterization of a Middle
788 Miocene Monogenetic Volcanic Field Buried in the Canterbury Basin, New Zealand – Part I.
789 EarthArXiv.

790 Bischoff, A.P., Nicol, A., Beggs, M., 2017. Stratigraphy of architectural elements in a buried
791 volcanic system and implications for hydrocarbon exploration. Interpretation 5, SK141-
792 SK159.

793 Bishop, D., Bradshaw, J., Landis, C., 1985. Provisional terrane map of South Island, New
794 Zealand.

795 Brown, A.R., 2011. Interpretation of three-dimensional seismic data. Society of Exploration
796 Geophysicists and American Association of Petroleum ….

797 Buntin, S., Malehmir, A., Koyi, H., Högdahl, K., Malinowski, M., Larsson, S.Å., Thybo, H.,
798 Juhlin, C., Korja, A., Górszczyk, A., 2019. Emplacement and 3D geometry of crustal-scale
799 saucer-shaped intrusions in the Fennoscandian Shield. Scientific Reports 9, 10498.

800 Calvès, G., Schwab, A.M., Huuse, M., Clift, P.D., Gaina, C., Jolley, D., Tabrez, A.R., Inam,
801 A., 2011. Seismic volcanostratigraphy of the western Indian rifted margin: The pre-Deccan
802 igneous province. Journal of Geophysical Research: Solid Earth 116.

803 Cassidy, J., Locke, C.A., 2010. The Auckland volcanic field, New Zealand: Geophysical
804 evidence for structural and spatio-temporal relationships. Journal of Volcanology and
805 Geothermal Research 195, 127-137.

806 Chenrai, P., Huuse, M., 2020. Sand injection and polygonal faulting in the Great South Basin,
807 New Zealand. Geological Society, London, Special Publications 493, SP493-2018-2107.

808 Chopra, S., Marfurt, K.J., 2012. Seismic attribute expression of differential compaction. The
809 Leading Edge 31, 1418-1422.

810 Clague, D.A., Jarrard, R.D., 1973. Tertiary Pacific Plate Motion Deduced from the Hawaiian-
811 Emperor Chain. GSA Bulletin 84, 1135-1154.

812 Clouard, V., Bonneville, A., 2005. Ages of seamounts, islands, and plateaus on the Pacific
813 plate. Special Papers-Geological Society of America 388, 71.

814 Collanega, L., Jackson, C.A.L., Bell, R.E., Coleman, A.J., Lenhart, A., Breda, A., 2018.
815 Normal fault growth influenced by basement fabrics: the importance of preferential
816 nucleation from pre-existing structures. Basin Res 0.

817 Cooper, A.F., Barreiro, B.A., Kimbrough, D.L., Mattinson, J.M., 1987. Lamprophyre dike
818 intrusion and the age of the Alpine fault, New Zealand. Geology 15, 941-944.

819 Cooper, A.F., Norris, R.J., 1994. Anatomy, structural evolution, and slip rate of a plate-
820 boundary thrust: The Alpine fault at Gaunt Creek, Westland, New Zealand. GSA Bulletin
821 106, 627-633.

822 Davey, F.J., Christoffel, D.A., 1978. Magnetic anomalies across Campbell Plateau, New
823 Zealand. Earth and Planetary Science Letters 41, 14-20.

824 Davies, D.R., Rawlinson, N., Iaffaldano, G., Campbell, I.H., 2015. Lithospheric controls on
825 magma composition along Earth's longest continental hotspot track. Nature 525, 511.

826 Davy, B., Hoernle, K., Werner, R., 2008. Hikurangi Plateau: Crustal structure, rifted
827 formation, and Gondwana subduction history. Geochemistry, Geophysics, Geosystems 9.

828 Eccles, J.D., Cassidy, J., Locke, C.A., Spörli, K.B., 2005. Aeromagnetic imaging of the Dun
829 Mountain Ophiolite Belt in northern New Zealand: insight into the fine structure of a major
830 SW Pacific terrane suture. Journal of the Geological Society 162, 723.

831 Eide, C.H., Schofield, N., Lecomte, I., Buckley, S.J., Howell, J.A., 2018. Seismic
832 interpretation of sill complexes in sedimentary basins: implications for the sub-sill imaging
833 problem. Journal of the Geological Society 175, 193-209.

834 Elkins-Tanton, L.T., 2005. Continental magmatism caused by lithospheric delamination, in:
835 Foulger, G.R., Natland, J.H., Presnall, D.C., Anderson, D.L. (Eds.), Plates, plumes and
836 paradigms. Geological Society of America, p. 0.

837 Finn, C.A., Müller, R.D., Panter, K.S., 2005. A Cenozoic diffuse alkaline magmatic province
838 (DAMP) in the southwest Pacific without rift or plume origin. Geochemistry, Geophysics,
839 Geosystems 6.

840 Fulthorpe, C.S., Carter, R.M., Miller, K.G., Wilson, J., 1996. Marshall Paraconformity: a
841 mid-Oligocene record of inception of the Antarctic circumpolar current and coeval glacio-
842 eustatic lowstand? Marine and Petroleum Geology 13, 61-77.

843 Galerne, C.Y., Galland, O., Neumann, E.-R., Planke, S., 2011. 3D relationships between sills
844 and their feeders: evidence from the Golden Valley Sill Complex (Karoo Basin) and
845 experimental modelling. Journal of Volcanology and Geothermal Research 202, 189-199.

846 Gallagher, J.W., Dromgoole, P.W., 2007. Exploring below the basalt, offshore Faroes: a case
847 history of sub-basalt imaging. Petroleum Geoscience 13, 213.

848 Grindley, G.W., Adams, C.J.D., Lumb, J.T., Watters, W.A., 1977. Paleomagnetism, K-Ar
849 dating and tectonic interpretation of Upper Cretaceous and Cenozoic volcanic rocks of the
850 Chatham Islands, New Zealand. New Zealand Journal of Geology and Geophysics 20, 425-
851 467.

852 Grobys, J.W.G., Gohl, K., Uenzelmann-Neben, G., Davy, B., Barker, D., 2009. Extensional
853 and magmatic nature of the Campbell Plateau and Great South Basin from deep crustal
854 studies. Tectonophysics 472, 213-225.

855 Hansen, D.M., Cartwright, J., 2006. The three-dimensional geometry and growth of forced
856 folds above saucer-shaped igneous sills. Journal of Structural Geology 28, 1520-1535.

857 Hansen, D.M., Redfern, J., Federici, F., di Biase, D., Bertozzi, G., 2008. Miocene igneous
858 activity in the Northern Subbasin, offshore Senegal, NW Africa. Marine and Petroleum
859 Geology 25, 1-15.

860 Higgs, K.E., Browne, G.H., Sahoo, T.R., 2019. Reservoir characterisation of syn-rift and
861 post-rift sandstones in frontier basins: An example from the Cretaceous of Canterbury and
862 Great South basins, New Zealand. Marine and Petroleum Geology 101, 1-29.

Hoernle, K., White, J.D.L., van den Bogaard, P., Hauff, F., Coombs, D.S., Werner, R., Timm, C., Garbe-Schönberg, D., Reay, A., Cooper, A.F., 2006. Cenozoic intraplate volcanism on New Zealand: Upwelling induced by lithospheric removal. Earth and Planetary Science Letters 248, 350-367.

Holford, S.P., Schofield, N., Reynolds, P., 2017. Subsurface fluid flow focused by buried volcanoes in sedimentary basins: Evidence from 3D seismic data, Bass Basin, offshore southeastern Australia. Interpretation 5, SK39-SK50.

Howell, D.G., 1980. Mesozoic accretion of exotic terranes along the New Zealand segment of Gondwanaland. Geology 8, 487-491.

Hunt, T., 1978. Stokes magnetic anomaly system. New Zealand journal of geology and geophysics 21, 595-606.

Jackson, C.A.L., 2012. Seismic reflection imaging and controls on the preservation of ancient sill-fed magmatic vents. Journal of the Geological Society 169, 503.

Johnston, M.R., 2019. Chapter 2 The path to understanding the central terranes of Zealandia. Geological Society, London, Memoirs 49, 15-30.

Kaislaniemi, L., van Hunen, J., Allen, M.B., Neill, I., 2014. Sublithospheric small-scale convection—A mechanism for collision zone magmatism. Geology 42, 291-294.

Kallweit, R.S., Wood, L.C., 1982. The limits of resolution of zero-phase wavelets. Geophysics 47, 1035-1046.

Kavanagh, J.L., Menand, T., Sparks, R.S.J., 2006. An experimental investigation of sill formation and propagation in layered elastic media. Earth and Planetary Science Letters 245, 799-813.

Kenny, J.A., Lindsay, J.M., Howe, T.M., 2012. Post-Miocene faults in Auckland: insights from borehole and topographic analysis. New Zealand Journal of Geology and Geophysics 55, 323-343.

Killops, S.D., Cook, R.A., Sykes, R., Boudou, J.P., 1997. Petroleum potential and oil-source correlation in the Great South and Canterbury Basins. New Zealand Journal of Geology and Geophysics 40, 405-423.

Kula, J., Tulloch, A., Spell, T.L., Wells, M.L., 2007. Two-stage rifting of Zealandia-Australia-Antarctica: Evidence from 40Ar/39Ar thermochronometry of the Sisters shear zone, Stewart Island, New Zealand. Geology 35, 411-414.

Laird, M.G., Bradshaw, J.D., 2004. The Break-up of a Long-term Relationship: the Cretaceous Separation of New Zealand from Gondwana. Gondwana Research 7, 273-286.

Lamb, S., Mortimer, N., Smith, E., Turner, G., 2016. Focusing of relative plate motion at a continental transform fault: Cenozoic dextral displacement >700 km on New Zealand's Alpine Fault, reversing >225 km of Late Cretaceous sinistral motion. Geochemistry, Geophysics, Geosystems 17, 1197-1213.

Ledevin, M., Arndt, N., Cooper, M.R., Earls, G., Lyle, P., Aubourg, C., Lewin, E., 2012. Intrusion history of the Portrush Sill, County Antrim, Northern Ireland: evidence for rapid emplacement and high-temperature contact metamorphism. Geological Magazine 149, 67-79.

Lindsay, J.M., Leonard, G.S., Smid, E.R., Hayward, B.W., 2011. Age of the Auckland Volcanic Field: a review of existing data. New Zealand Journal of Geology and Geophysics 54, 379-401.

Lu, H., Fulthorpe, C.S., 2004. Controls on sequence stratigraphy of a middle Miocene–Holocene, current-swept, passive margin: Offshore Canterbury Basin, New Zealand. GSA Bulletin 116, 1345-1366.

Magee, C., Briggs, F., Jackson, C.A.L., 2013a. Lithological controls on igneous intrusion-induced ground deformation. Journal of the Geological Society 170, 853.

Magee, C., Ernst, R.E., Muirhead, J., Phillips, T., Jackson, C.A.-L., 2019. Magma Transport Pathways in Large Igneous Provinces: Lessons from Combining Field Observations and Seismic Reflection Data, Dyke Swarms of the World: A Modern Perspective. Springer, pp. 45-85.

Magee, C., Hunt-Stewart, E., Jackson, C.A.L., 2013b. Volcano growth mechanisms and the role of sub-volcanic intrusions: Insights from 2D seismic reflection data. Earth and Planetary Science Letters 373, 41-53.

Magee, C., Jackson, C.A.-L., How do normal faults grow above dykes? EarthArXiv.

Magee, C., Jackson, C.A.L., 2020. Seismic reflection data reveal the 3D structure of the newly discovered Exmouth Dyke Swarm, offshore NW Australia. EarthArXiv.

Magee, C., Jackson, C.A.L., Hardman, J.P., Reeve, M.T., 2017. Decoding sill emplacement and forced fold growth in the Exmouth Sub-basin, offshore northwest Australia: Implications for hydrocarbon exploration. Interpretation 5, SK11-SK22.

Magee, C., Muirhead, J.D., Karvelas, A., Holford, S.P., Jackson, C.A.L., Bastow, I.D., Schofield, N., Stevenson, C.T.E., McLean, C., McCarthy, W., Shtukert, O., 2016. Lateral magma flow in mafic sill complexes. Geosphere 12, 809-841.

Magee, C., Stevenson, C.T.E., Ebmeier, S.K., Keir, D., Hammond, J.O.S., Gottsmann, J.H., Whaler, K.A., Schofield, N., Jackson, C.A.L., Petronis, M.S., O'Driscoll, B., Morgan, J., Cruden, A., Vollgger, S.A., Dering, G., Micklethwaite, S., Jackson, M.D., 2018. Magma Plumbing Systems: A Geophysical Perspective. Journal of Petrology 59, 1217-1251.

931 Maresh, J., White, R.S., Hobbs, R.W., Smallwood, J.R., 2006. Seismic attenuation of Atlantic
932 margin basalts: Observations and modeling. Geophysics 71, B211-B221.

933 Mazzarini, F., 2007. Vent distribution and crustal thickness in stretched continental crust: The
934 case of the Afar Depression (Ethiopia). Geosphere 3, 152-162.

935 McGee, L.E., Smith, I.E.M., Millet, M.-A., Handley, H.K., Lindsay, J.M., 2013.
936 Asthenospheric Control of Melting Processes in a Monogenetic Basaltic System: a Case
937 Study of the Auckland Volcanic Field, New Zealand. Journal of Petrology 54, 2125-2153.

938 McLean, C.E., Schofield, N., Brown, D.J., Jolley, D.W., Reid, A., 2017. 3D seismic imaging
939 of the shallow plumbing system beneath the Ben Nevis Monogenetic Volcanic Field: Faroe–
940 Shetland Basin. Journal of the Geological Society 174, 468.

941 Morewood, N.C., Shannon, P.M., Mackenzie, G.D., 2004. Seismic stratigraphy of the
942 southern Rockall Basin: a comparison between wide-angle seismic and normal incidence
943 reflection data. Marine and Petroleum Geology 21, 1149-1163.

944 Morgan, W.J., 1972. Deep mantle convection plumes and plate motions. AAPG bulletin 56,
945 203-213.

946 Morley, C.K., 2018. 3-D seismic imaging of the plumbing system of the Kora Volcano,
947 Taranaki Basin, New Zealand: The influence of syn-rift structure on shallow igneous
948 intrusion architecture. Geosphere 14, 2533-2584.

949 Morley, C.K., Maczak, A., Rungprom, T., Ghosh, J., Cartwright, J.A., Bertoni, C.,
950 Panpichityota, N., 2017. New style of honeycomb structures revealed on 3D seismic data
951 indicate widespread diagenesis offshore Great South Basin, New Zealand. Marine and
952 Petroleum Geology 86, 140-154.

953 Mortimer, N., 2004. New Zealand's Geological Foundations. Gondwana Research 7, 261-
954 272.

955 Mortimer, N., Davey, F.J., Melhuish, A., Yu, J., Godfrey, N.J., 2002. Geological
956 interpretation of a deep seismic reflection profile across the Eastern Province and Median
957 Batholith, New Zealand: Crustal architecture of an extended Phanerozoic convergent orogen.
958 New Zealand Journal of Geology and Geophysics 45, 349-363.

959 Mortimer, N., Rattenbury, M.S., King, P.R., Bland, K.J., Barrell, D.J.A., Bache, F., Begg,
960 J.G., Campbell, H.J., Cox, S.C., Crampton, J.S., Edbrooke, S.W., Forsyth, P.J., Johnston,
961 M.R., Jongens, R., Lee, J.M., Leonard, G.S., Raine, J.I., Skinner, D.N.B., Timm, C.,
962 Townsend, D.B., Tulloch, A.J., Turnbull, I.M., Turnbull, R.E., 2014. High-level stratigraphic
963 scheme for New Zealand rocks. New Zealand Journal of Geology and Geophysics 57, 402-
964 419.

965 Mortimer, N., Tulloch, A.J., Spark, R.N., Walker, N.W., Ladley, E., Allibone, A.,
966 Kimbrough, D.L., 1999. Overview of the Median Batholith, New Zealand: a new

967 interpretation of the geology of the Median Tectonic Zone and adjacent rocks. Journal of
968 African Earth Sciences 29, 257-268.

969 Mortimer, N., van den Bogaard, P., Hoernle, K., Timm, C., Gans, P.B., Werner, R., Riefstahl,
970 F., 2019. Late Cretaceous oceanic plate reorganization and the breakup of Zealandia and
971 Gondwana. Gondwana Research 65, 31-42.

972 Muir, R.J., Bradshaw, J.D., Weaver, S.D., Laird, M.G., 2000. The influence of basement
973 structure on the evolution of the Taranaki Basin, New Zealand. Journal of the Geological
974 Society 157, 1179.

975 Németh, K., 2010. Monogenetic volcanic fields: Origin, sedimentary record, and relationship
976 with polygenetic volcanism, in: Cañón-Tapia, E., Szakács, A. (Eds.), What Is a Volcano?
977 Geological Society of America, p. 0.

978 Németh, K., White, J.D.L., 2003. Reconstructing eruption processes of a Miocene
979 monogenetic volcanic field from vent remnants: Waipiata Volcanic Field, South Island, New
980 Zealand. Journal of Volcanology and Geothermal Research 124, 1-21.

981 Németh, K., White, J.D.L., Reay, A., Martin, U., 2003. Compositional variation during
982 monogenetic volcano growth and its implications for magma supply to continental volcanic
983 fields. Journal of the Geological Society 160, 523.

984 Patruno, S., Helland-Hansen, W., 2018. Clinoforms and clinoform systems: Review and
985 dynamic classification scheme for shorelines, subaqueous deltas, shelf edges and continental
986 margins. Earth-Science Reviews 185, 202-233.

987 Phillips, T.B., McCaffrey, K.J., 2019. Terrane boundary reactivation, barriers to lateral fault
988 propagation and reactivated fabrics - Rifting across the Median Batholith Zone, Great South
989 Basin, New Zealand. Tectonics 0.

990 Planke, S., Rasmussen, T., Rey, S.S., Myklebust, R., 2005. Seismic characteristics and
991 distribution of volcanic intrusions and hydrothermal vent complexes in the Vøring and Møre
992 basins. Geological Society, London, Petroleum Geology Conference
993 series 6, 833.

994 Planke, S., Symonds, P.A., Alvestad, E., Skogseid, J., 2000. Seismic volcanostratigraphy of
995 large-volume basaltic extrusive complexes on rifted margins. Journal of Geophysical
996 Research: Solid Earth 105, 19335-19351.

997 Polteau, S., Ferré, E.C., Planke, S., Neumann, E.R., Chevallier, L., 2008. How are saucer-
998 shaped sills emplaced? Constraints from the Golden Valley Sill, South Africa. Journal of
999 Geophysical Research: Solid Earth 113.

1000 Price, R., Chappell, B., 1975. Fractional crystallisation and the petrology of Dunedin
1001 Volcano. Contributions to mineralogy and petrology 53, 157-182.

1002 Pryer, L., Weir, J., Debacker, T., Romine, K., 2013. Interpretation of basement: NZ ECS
1003 SEEBASE: Advantage New Zealand Petroleum Summit. April.

1004 Quirie, A.K., Schofield, N., Hartley, A., Hole, M.J., Archer, S.G., Underhill, J.R., Watson,
1005 D., Holford, S.P., 2019. The Rattray Volcanics: Mid-Jurassic fissure volcanism in the UK
1006 Central North Sea. Journal of the Geological Society 176, 462-481.

1007 Rawlinson, N., Davies, D.R., Pilia, S., 2017. The mechanisms underpinning Cenozoic
1008 intraplate volcanism in eastern Australia: Insights from seismic tomography and geodynamic
1009 modeling. Geophysical Research Letters 44, 9681-9690.

1010 Reeves, J., Magee, C., Jackson, C., 2018. Unravelling intrusion-induced forced fold
1011 kinematics and ground deformation using 3D seismic reflection data. Volcanica, 1-17.

1012 Reynolds, P., Holford, S., Schofield, N., Ross, A., 2017. Three-Dimensional Seismic Imaging
1013 of Ancient Submarine Lava Flows: An Example From the Southern Australian Margin.
1014 Geochemistry, Geophysics, Geosystems 18, 3840-3853.

1015 Reynolds, P., Schofield, N., Brown, R.J., Holford, S.P., 2018. The architecture of submarine
1016 monogenetic volcanoes – insights from 3D seismic data. Basin Res 30, 437-451.

1017 Robertson, A.H.F., Campbell, H.J., Johnston, M.R., Palamakumbra, R., 2019. Chapter 15
1018 Construction of a Paleozoic–Mesozoic accretionary orogen along the active continental
1019 margin of SE Gondwana (South Island, New Zealand): summary and overview. Geological
1020 Society, London, Memoirs 49, 331-372.

1021 Rout, D.J., Cassidy, J., Locke, C.A., Smith, I.E.M., 1993. Geophysical evidence for temporal
1022 and structural relationships within the monogenetic basalt volcanoes of the Auckland
1023 volcanic field, northern New Zealand. Journal of Volcanology and Geothermal Research 57,
1024 71-83.

1025 Sahoo, T., King, P., Bland, K., Strogen, D., Sykes, R., Bache, F., 2014. Tectono-sedimentary
1026 evolution and source rock distribution of the mid to Late Cretaceous succession in the Great
1027 South Basin, New Zealand The APPEA Journal 54, 259-274.

1028 Slatt, R.M., 2006. Stratigraphic reservoir characterization for petroleum geologists,
1029 geophysicists, and engineers. Elsevier.

1030 Sleep, N.H., 1992. Hotspot volcanism and mantle plumes. Annual Review of Earth and
1031 Planetary Sciences 20, 19-43.

1032 Smallwood, J.R., Maresh, J., 2002. The properties, morphology and distribution of igneous
1033 sills: modelling, borehole data and 3D seismic from the Faroe-Shetland area. Geological
1034 Society, London, Special Publications 197, 271.

1035 Speight, R., 1943. The geology of Banks Peninsula: a revision, Transactions of the New
1036 Zealand Institute, pp. 13-26.

1037 Spörli, K.B., Black, P.M., Lindsay, J.M., 2015. Excavation of buried Dun Mountain–Maitai
1038 terrane ophiolite by volcanoes of the Auckland Volcanic field, New Zealand. New Zealand
1039 Journal of Geology and Geophysics 58, 229-243.

1040 Spörli, K.B., Eastwood, V.R., 1997. Elliptical boundary of an intraplate volcanic field,
1041 Auckland, New Zealand. Journal of Volcanology and Geothermal Research 79, 169-179.

1042 Stephens, T.L., Walker, R.J., Healy, D., Bubeck, A., England, R.W., McCaffrey, K.J.W.,
1043 2017. Igneous sills record far-field and near-field stress interactions during volcano
1044 construction: Isle of Mull, Scotland. Earth and Planetary Science Letters 478, 159-174.

1045 Stipp, J.J., McDougall, I., 1968. Geochronology of the Banks Peninsula Volcanoes, New
1046 Zealand. New Zealand Journal of Geology and Geophysics 11, 1239-1258.

1047 Sun, Q., Jackson, C.A.L., Magee, C., Mitchell, S.J., Xie, X., 2019a. Extrusion dynamics of
1048 deep-water volcanoes. Solid Earth Discuss. 2019, 1-40.

1049 Sun, Q., Jackson, C.A.L., Magee, C., Xie, X., 2019b. Deeply buried ancient volcanoes
1050 control hydrocarbon migration in the South China Sea. Basin Res n/a.

1051 Sutherland, R., 1995. The Australia-Pacific boundary and Cenozoic plate motions in the SW
1052 Pacific: Some constraints from Geosat data. Tectonics 14, 819-831.

1053 Sutherland, R., 1999. Basement geology and tectonic development of the greater New
1054 Zealand region: an interpretation from regional magnetic data. Tectonophysics 308, 341-362.

1055 Symonds, P.A., Planke, S., Frey, O., Skogseid, J., 1998. Volcanic evolution of the Western
1056 Australian continental margin and its implications for basin development.

1057 Tarling, M.S., Smith, S.A.F., Scott, J.M., Rooney, J.S., Viti, C., Gordon, K.C., 2019. The
1058 internal structure and composition of a plate-boundary-scale serpentinite shear zone: the
1059 Livingstone Fault, New Zealand. Solid Earth 10, 1025-1047.

1060 Thomson, K., 2005. Volcanic features of the North Rockall Trough: application of
1061 visualisation techniques on 3D seismic reflection data. Bulletin of Volcanology 67, 116-128.

1062 Thomson, K., Hutton, D., 2004. Geometry and growth of sill complexes: insights using 3D
1063 seismic from the North Rockall Trough. Bulletin of Volcanology 66, 364-375.

1064 Timm, C., Hoernle, K., Van Den Bogaard, P., Bindeman, I., Weaver, S., 2009. Geochemical
1065 Evolution of Intraplate Volcanism at Banks Peninsula, New Zealand: Interaction Between
1066 Asthenospheric and Lithospheric Melts. Journal of Petrology 50, 989-1023.

1067 Timm, C., Hoernle, K., Werner, R., Hauff, F., den Bogaard, P.v., White, J., Mortimer, N.,
1068 Garbe-Schönberg, D., 2010. Temporal and geochemical evolution of the Cenozoic intraplate
1069 volcanism of Zealandia. Earth-Science Reviews 98, 38-64.

1070 Trude, J., Cartwright, J., Davies, R.J., Smallwood, J., 2003. New technique for dating igneous
1071 sills. Geology 31, 813-816.

1072 Tulloch, A., Mortimer, N., Ireland, T., Waight, T., Maas, R., Palin, M., Sahoo, T., Seebeck,
1073 H., Sagar, M., Barrier, A., Turnbull, R., 2019. Reconnaissance basement geology and
1074 tectonics of South Zealandia. Tectonics 0.

1075 Uruski, C., 2015. The contribution of offshore seismic data to understanding the evolution of
1076 the New Zealand continent. Geol Soc Spec Publ 413, 35-51.

1077 Uruski, C., Kennedy, C., Harrison, T., Maslen, G., Cook, R., Sutherland, R., Zhu, H., 2007.
1078 Petroleum potential of the Great South Basin, New Zealand—New seismic data improves
1079 imaging. The APPEA Journal 47, 145-161.

1080 Uruski, C.I., 2010. New Zealand's deepwater frontier. Marine and Petroleum Geology 27,
1081 2005-2026.

1082 Valentine, G.A., Hirano, N., 2010. Mechanisms of low-flux intraplate volcanic fields—Basin
1083 and Range (North America) and northwest Pacific Ocean. Geology 38, 55-58.

1084 Waight, T.E., Weaver, S.D., Maas, R., Eby, G.N., 1998. French Creek Granite and Hohonu
1085 Dyke Swarm, South Island, New Zealand: Late Cretaceous alkaline magmatism and the
1086 opening of the Tasman Sea. Australian Journal of Earth Sciences 45, 823-835.

1087 Walker, F., Schofield, N., Millett, J., Jolley, D., Hole, M., Stewart, M., 2019. Paleogene
1088 volcanic rocks in the northern Faroe-Shetland Basin and Møre Marginal High: Understanding
1089 lava field stratigraphy. Geological Society, London, Special Publications 495, SP495-2019-
1090 2013.

1091 Wall, M., Cartwright, J., Davies, R., McGrandle, A., 2010. 3D seismic imaging of a Tertiary
1092 Dyke Swarm in the Southern North Sea, UK. Basin Res 22, 181-194.

1093 Widess, M.B., 1973. How thin is a thin bed? Geophysics 38, 1176-1180.

1094 Wilson, C., Houghton, B., McWilliams, M., Lanphere, M., Weaver, S., Briggs, R., 1995.
1095 Volcanic and structural evolution of Taupo Volcanic Zone, New Zealand: a review. Journal
1096 of volcanology and geothermal research 68, 1-28.

1097 Woodward, D., Hatherton, T., 1975. Magnetic anomalies over southern New Zealand. New
1098 Zealand journal of geology and geophysics 18, 65-82.

1099 Wright, K.A., Davies, R.J., Jerram, D.A., Morris, J., Fletcher, R., 2012. Application of
1100 seismic and sequence stratigraphic concepts to a lava-fed delta system in the Faroe-Shetland
1101 Basin, UK and Faroes. Basin Res 24, 91-106.

1102 Wright, N.M., Seton, M., Williams, S.E., Müller, R.D., 2016. The Late Cretaceous to recent
1103 tectonic history of the Pacific Ocean basin. Earth-Science Reviews 154, 138-173.

1104 Wu, L., Mei, L., Paton, D.A., Guo, P., Liu, Y., Luo, J., Wang, D., Li, M., Zhang, P., Wen, H.,
1105 2018. Deciphering the origin of the Cenozoic intracontinental rifting and volcanism in eastern
1106 China using integrated evidence from the Jianghan Basin. Gondwana Research 64, 67-83.

1107 Zhao, F., Wu, S., Sun, Q., Huuse, M., Li, W., Wang, Z., 2014. Submarine volcanic mounds in
1108 the Pearl River Mouth Basin, northern South China Sea. Marine Geology 355, 162-172.

1109

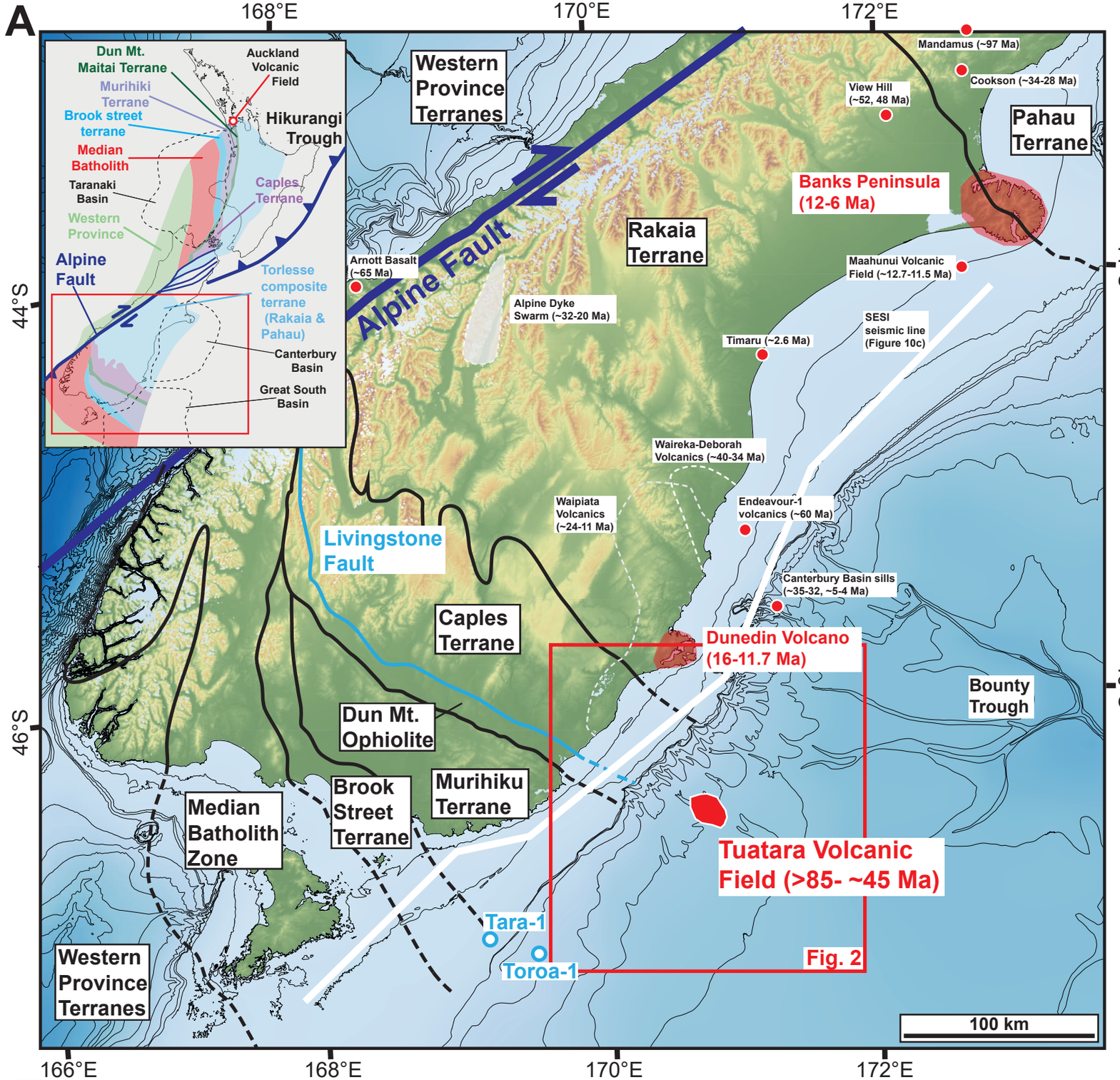
A
168°E
170°E
172°E
44°S
49°S
Dun Mt.
Maitai Terrane
Murihiki
Terrane
Brook street
terrane
Median
Batholith
Taranaki
Basin
Western
Province
Alpine
Fault
Auckland
Volcanic
Field
Hikurangi
Trough
Caples
Terrane
Torlesse
composite
terrane
(Rakaia &
Pahau)
Canterbury
Basin
Great South
Basin
Western
Province
Terranes
Alpine Fault
Rakaia
Terrane
Pahau
Terrane
Banks Peninsula
(12-6 Ma)
Mandamus (~97 Ma)
Cookson (~34-28 Ma)
View Hill
(~52, 48 Ma)
Arnott Basalt
(~65 Ma)
Alpine Dyke
Swarm (~32-20 Ma)
Maahunui Volcanic
Field (~12.7-11.5 Ma)
SESI
seismic line
(Figure 10c)
Timaru (~2.6 Ma)
Waireka-Deborah
Volcanics (~40-34 Ma)
Waipiata
Volcanics
(~24-11 Ma)
Endeavour-1
volcanics (~60 Ma)
Canterbury Basin sills
(~35-32, ~5-4 Ma)
Livingstone
Fault
Caples
Terrane
Dunedin Volcano
(16-11.7 Ma)
Bounty
Trough
Dun Mt.
Ophiolite
Brook
Street
Terrane
Murihiku
Terrane
Median
Batholith
Zone
Tuatara Volcanic
Field (>85- ~45 Ma)
Tara-1
Toroa-1
Fig. 2
Western
Province
Terranes
100 km
166°E
168°E
170°E
172°E
44°S
49°S

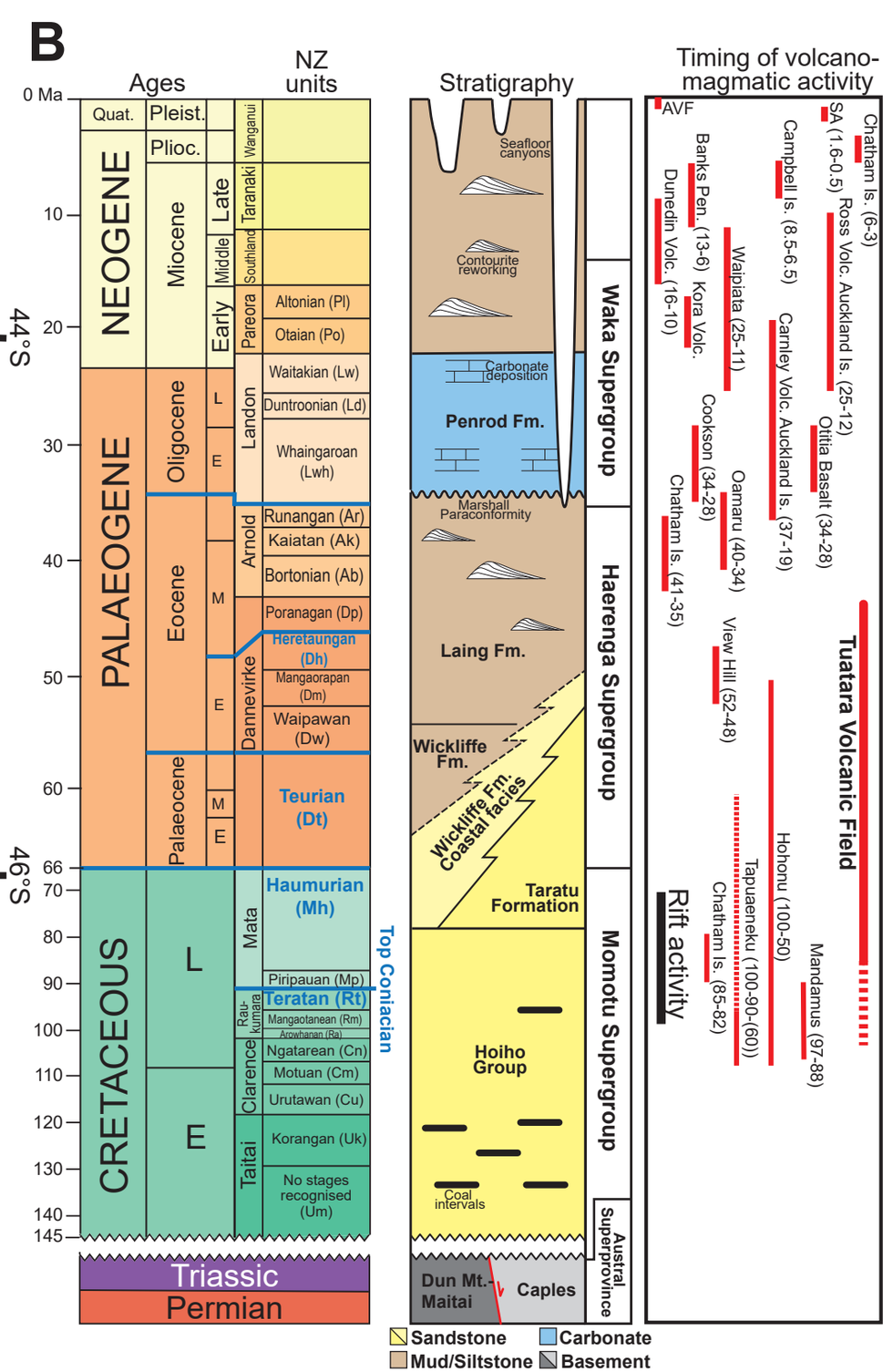
B
Ages
NZ units
Stratigraphy
Timing of volcano-magmatic activity
0 Ma
10
20
30
40
50
60
66
70
80
90
100
110
120
130
140
145
Quat.
Pleist.
Plioc.
NEOGENE
Miocene
Late
Middle
Early
PALAEOGENE
Oligocene
Eocene
Palaeocene
L
E
M
E
M
E
Wanganui
Taranaki
Southland
Pareora
Landon
Arnold
Dannevirke
Altonian (Pl)
Otaian (Po)
Waitakian (Lw)
Duntroonian (Ld)
Whaingaroan
(Lwh)
Runangan (Ar)
Kaiatan (Ak)
Bortonian (Ab)
Poranagan (Dp)
Heretaungan
(Dh)
Mangaorapan
(Dm)
Waipawan
(Dw)
Teurian
(Dt)
Top Coniacian
CRETACEOUS
L
E
Mata
Rau-
kumara
Clarence
Taitai
Haumurian
(Mh)
Piripauan (Mp)
Teratan (Rt)
Mangaotanean (Rm)
Arowhanan (Ra)
Ngatarean (Cn)
Motuan (Cm)
Urutawan (Cu)
Korangan (Uk)
No stages
recognised
(Um)
Triassic
Permian
Seafloor
canyons
Contourite
reworking
Carbonate
deposition
Penrod Fm.
Marshall
Paraconformity
Laing Fm.
Wickliffe
Fm.
Wickliffe Fm.
Coastal facies
Taratu
Formation
Hoiho
Group
Coal
intervals
Dun Mt.-
Maitai
Caples
Waka Supergroup
Haerenga Supergroup
Momotu Supergroup
Austral
Superprovince
AVF
Dunedin Volc. (16-10)
Banks Pen. (13-6)
Kora Volc.
Campbell Is. (8.5-6.5)
Waipiata (25-11)
Carnley Volc. Auckland Is. (37-19)
SA (1.6-0.5)
Ross Volc. Auckland Is. (25-12)
Chatham Is. (6-3)
Ottita Basalt (34-28)
Cookson (34-28)
Oamaru (40-34)
Chatham Is. (41-35)
View Hill (52-48)
Tuatara Volcanic Field
Hohonu (100-50)
Tapuaeneku (100-90-(60))
Chatham Is. (85-82)
Mandamus (97-88)
Rift activity
Sandstone
Carbonate
Mud/Siltstone
Basement

Figure 1

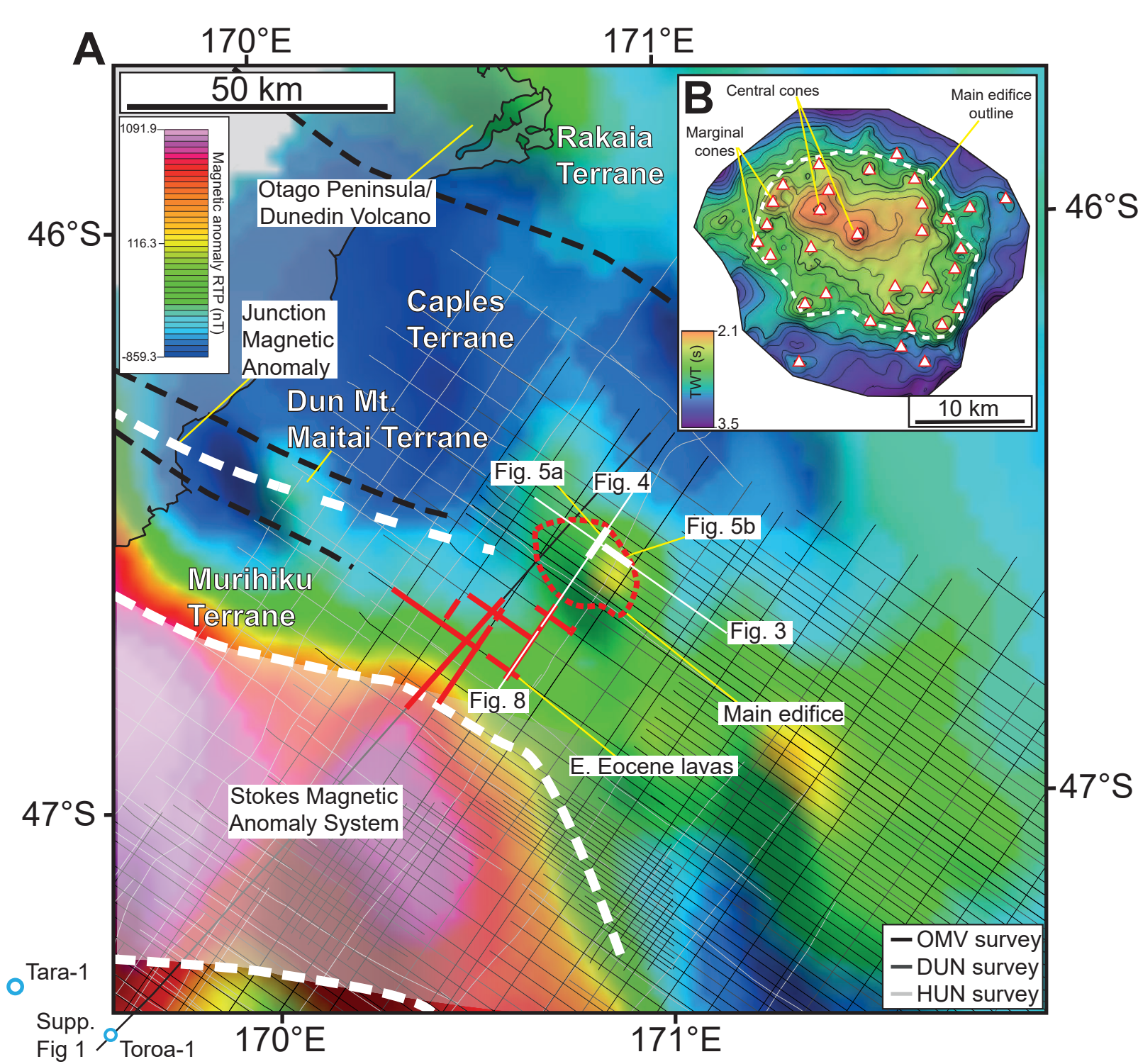
A
170°E
171°E
46°S
47°S
50 km
1091.9
116.3
-859.3
Magnetic anomaly RTP (nT)
Rakaia Terrane
Otago Peninsula/ Dunedin Volcano
Junction Magnetic Anomaly
Caples Terrane
Dun Mt. Maitai Terrane
Murihiku Terrane
Stokes Magnetic Anomaly System
Fig. 5a
Fig. 4
Fig. 5b
Fig. 3
Fig. 8
Main edifice
E. Eocene lavas
B
Central cones
Main edifice outline
Marginal cones
2.1
3.5
TWT (s)
10 km
OMV survey
DUN survey
HUN survey
Tara-1
Supp. Fig 1
Toroa-1

Figure 2

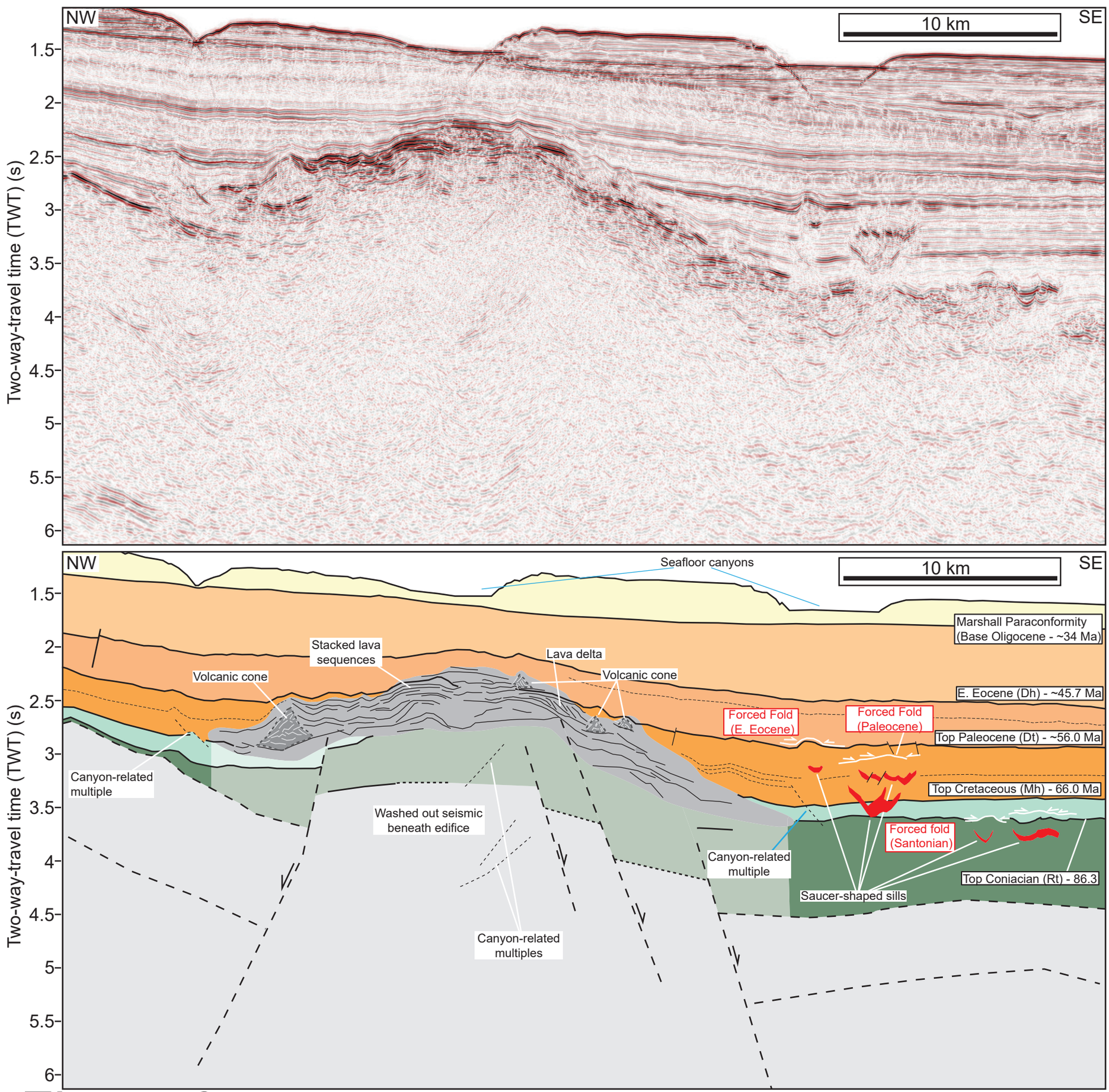
NW
SE
10 km
Two-way-travel time (TWT) (s)
1.5
2
2.5
3
3.5
4
4.5
5
5.5
6
Seafloor canyons
Marshall Paraconformity
(Base Oligocene - ~34 Ma)
Stacked lava
sequences
Lava delta
Volcanic cone
Volcanic cone
E. Eocene (Dh) - ~45.7 Ma
Forced Fold
(E. Eocene)
Forced Fold
(Paleocene)
Top Paleocene (Dt) - ~56.0 Ma
Canyon-related
multiple
Top Cretaceous (Mh) - 66.0 Ma
Washed out seismic
beneath edifice
Forced fold
(Santonian)
Canyon-related
multiple
Top Coniacian (Rt) - 86.3
Saucer-shaped sills
Canyon-related
multiples

Figure 3

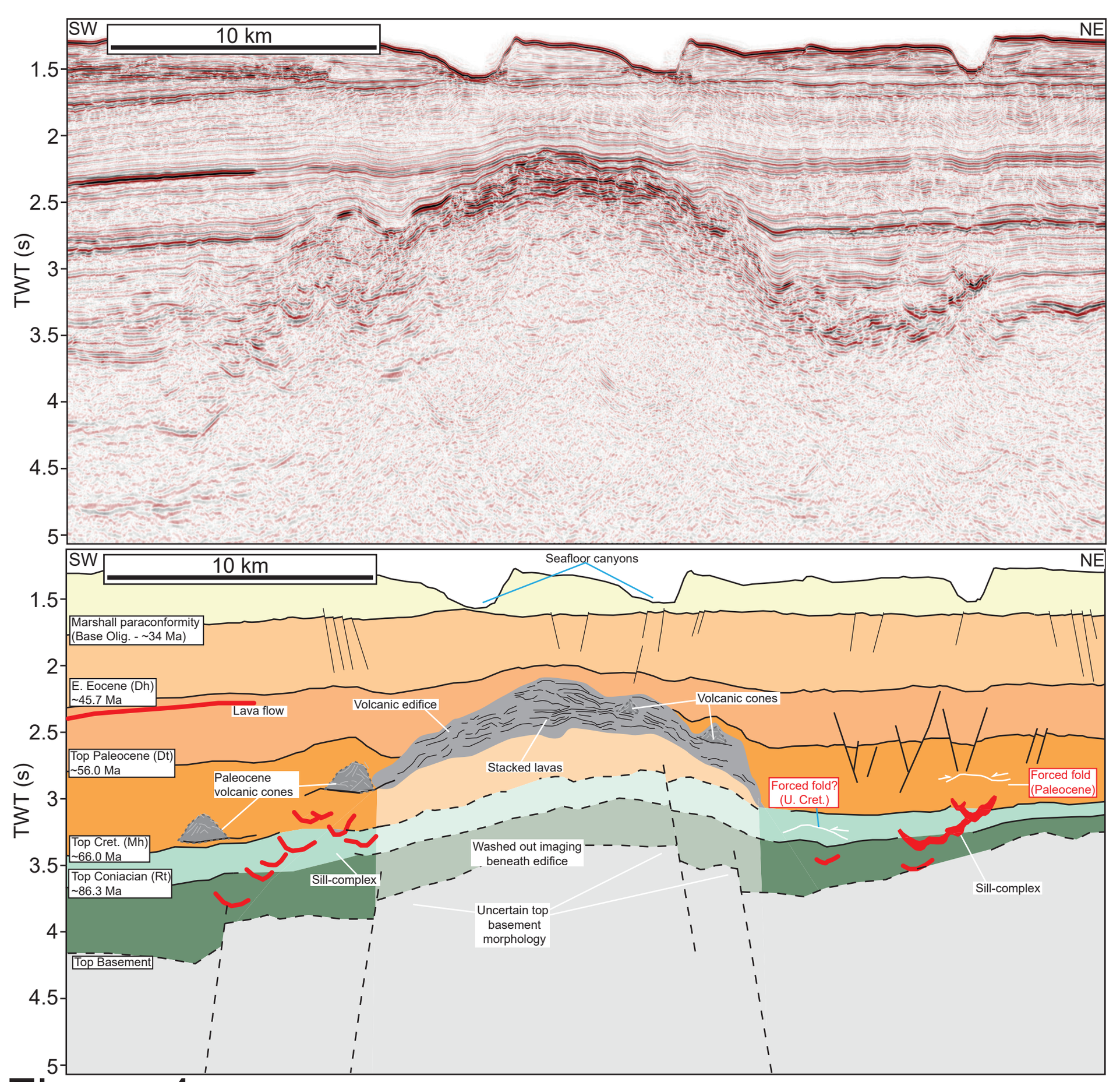
SW
10 km
NE
TWT (s)
1.5
2
2.5
3
3.5
4
4.5
5
SW
10 km
NE
Seafloor canyons
Marshall paraconformity
(Base Olig. - ~34 Ma)
E. Eocene (Dh)
~45.7 Ma
Lava flow
Volcanic edifice
Volcanic cones
Top Paleocene (Dt)
~56.0 Ma
Paleocene
volcanic cones
Stacked lavas
Forced fold?
(U. Cret.)
Forced fold
(Paleocene)
Top Cret. (Mh)
~66.0 Ma
Washed out imaging
beneath edifice
Top Coniacian (Rt)
~86.3 Ma
Sill-complex
Sill-complex
Uncertain top
basement
morphology
Top Basement

Figure 4

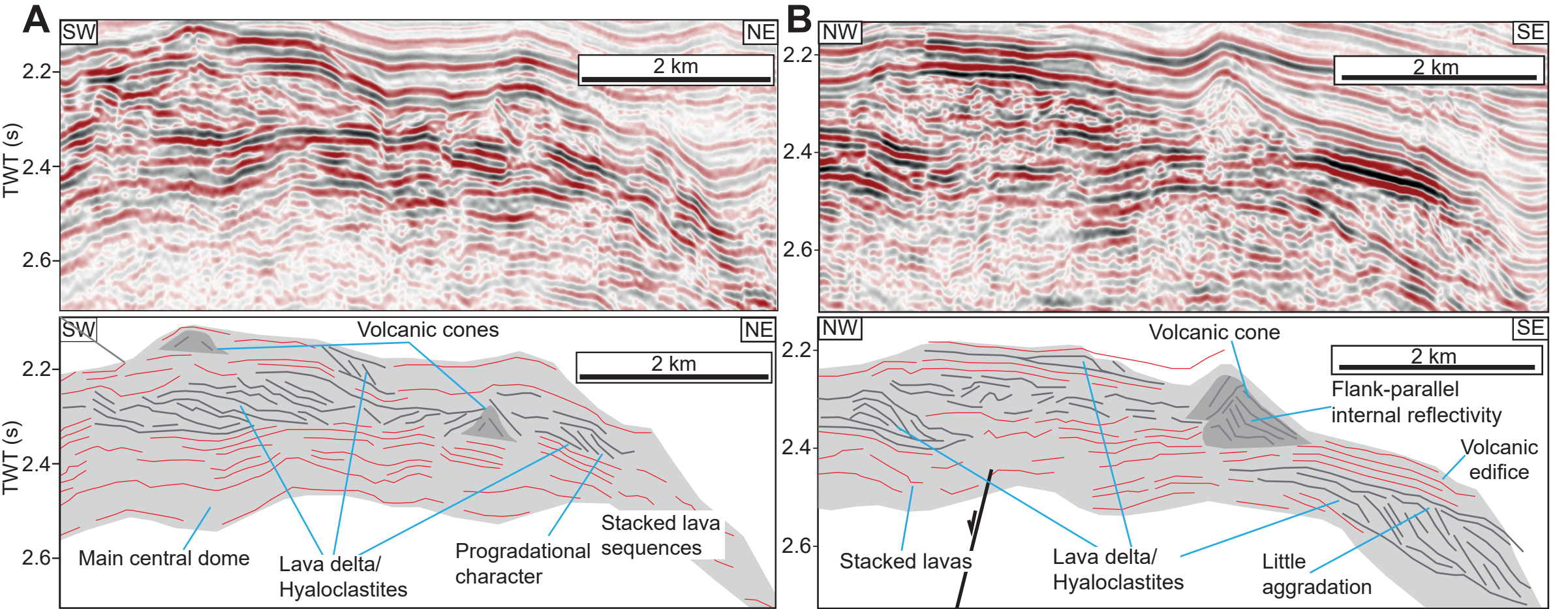
A
SW
NE
2 km
2.2
2.4
2.6
TWT (s)
B
NW
SE
2 km
2.2
2.4
2.6
SW
NE
Volcanic cones
2 km
2.2
2.4
2.6
TWT (s)
Main central dome
Lava delta/
Hyaloclastites
Progradational
character
Stacked lava
sequences
NW
SE
Volcanic cone
2 km
Flank-parallel
internal reflectivity
Volcanic
edifice
Stacked lavas
Lava delta/
Hyaloclastites
Little
aggradation

Figure 5

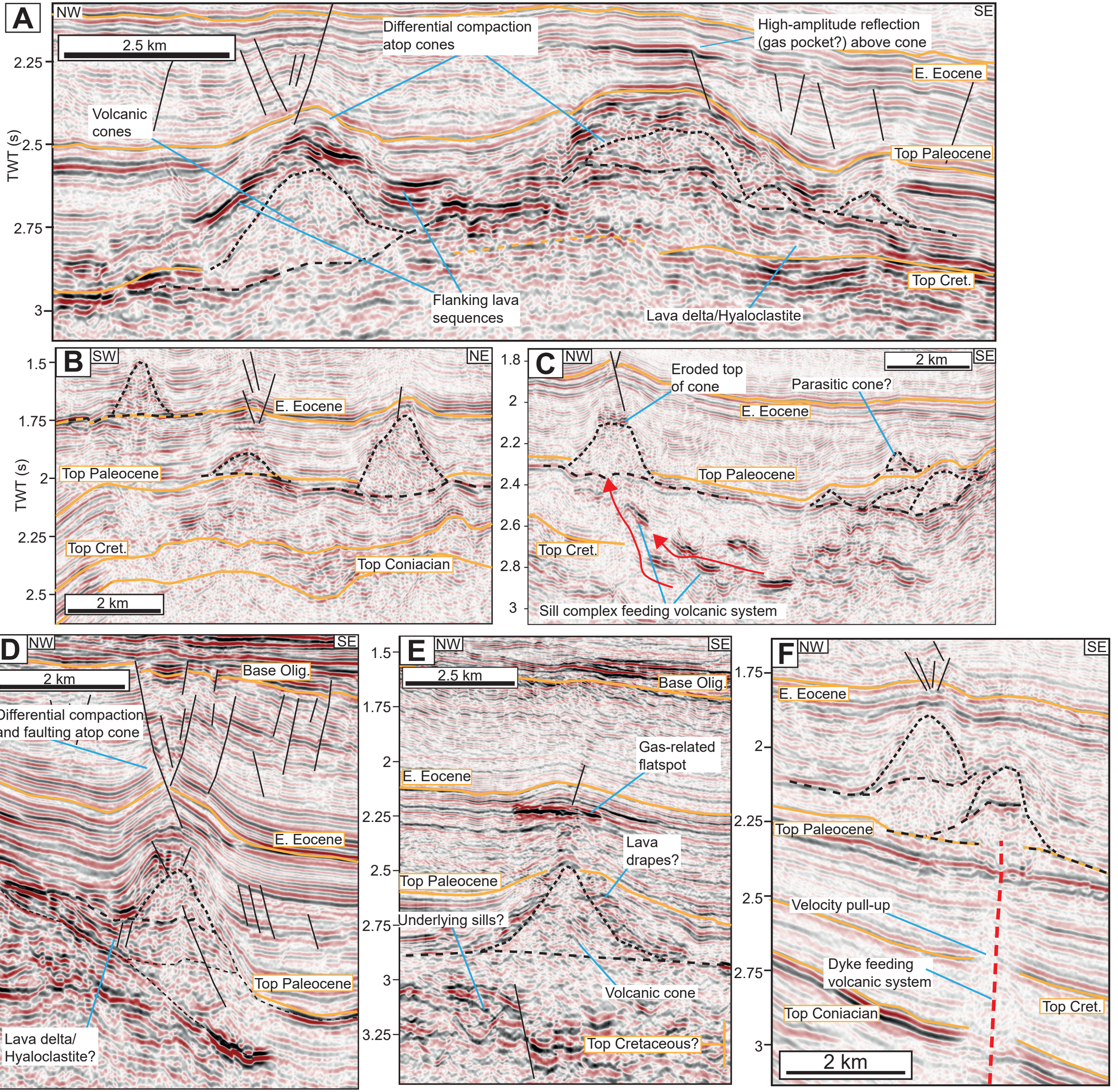
A
NW
SE
2.5 km
Differential compaction atop cones
High-amplitude reflection (gas pocket?) above cone
E. Eocene
Volcanic cones
Top Paleocene
TWT (s)
Top Cret.
Flanking lava sequences
Lava delta/Hyaloclastite
B
SW
NE
E. Eocene
Top Paleocene
Top Cret.
Top Coniacian
2 km
C
NW
SE
2 km
Eroded top of cone
Parasitic cone?
E. Eocene
Top Paleocene
Top Cret.
Sill complex feeding volcanic system
D
NW
SE
2 km
Base Olig.
Differential compaction and faulting atop cone
E. Eocene
Top Paleocene
Lava delta/ Hyaloclastite?
E
NW
SE
2.5 km
Base Olig.
Gas-related flatspot
E. Eocene
Lava drapes?
Top Paleocene
Underlying sills?
Volcanic cone
Top Cretaceous?
F
NW
SE
E. Eocene
Top Paleocene
Velocity pull-up
Dyke feeding volcanic system
Top Coniacian
Top Cret.
2 km

Figure 6

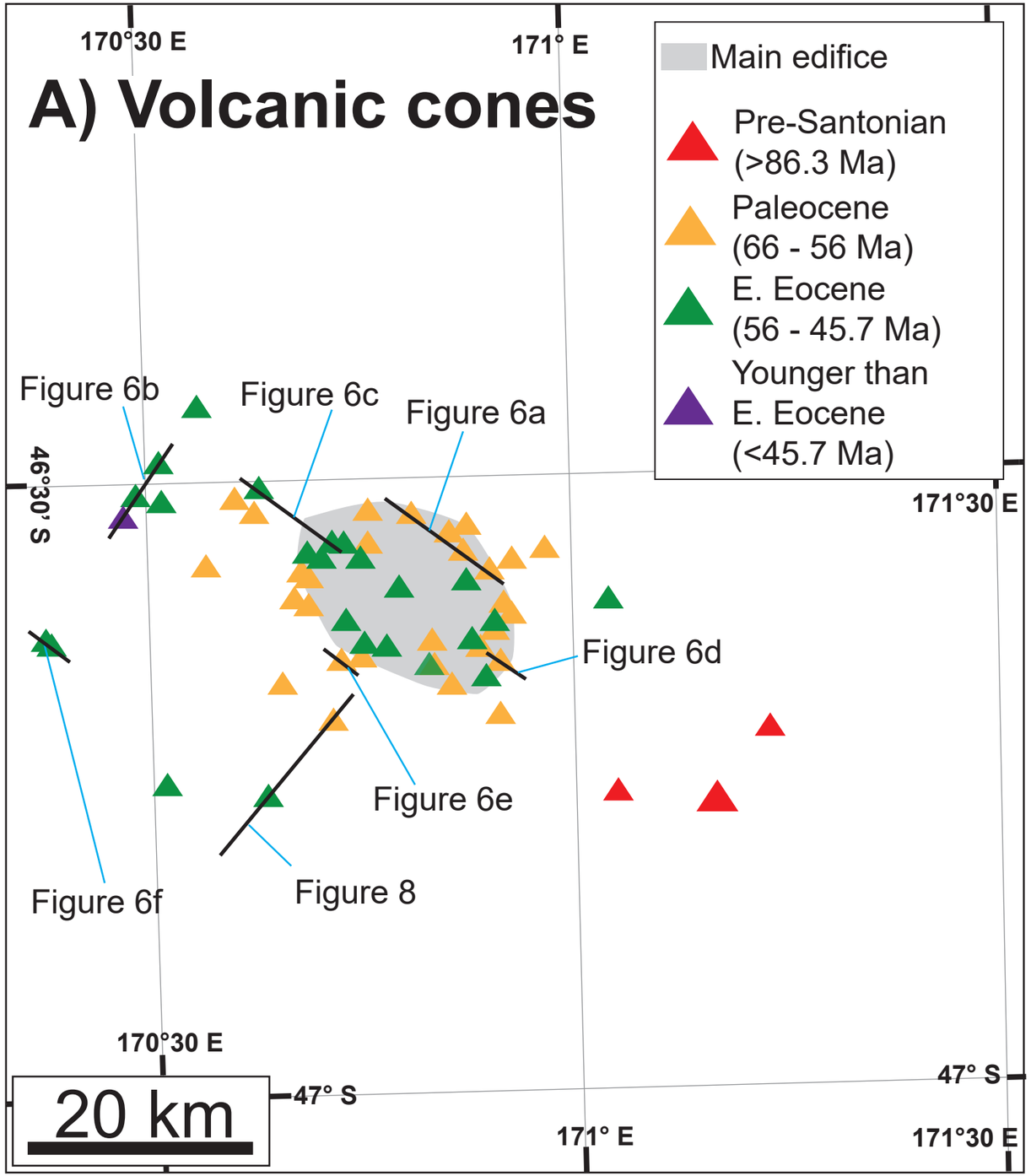
A) Volcanic cones
170°30 E
171° E
171°30 E
46°30' S
47° S
Main edifice
Pre-Santonian (>86.3 Ma)
Paleocene (66 - 56 Ma)
E. Eocene (56 - 45.7 Ma)
Younger than E. Eocene (<45.7 Ma)
Figure 6b
Figure 6c
Figure 6a
Figure 6d
Figure 6e
Figure 6f
Figure 8
20 km

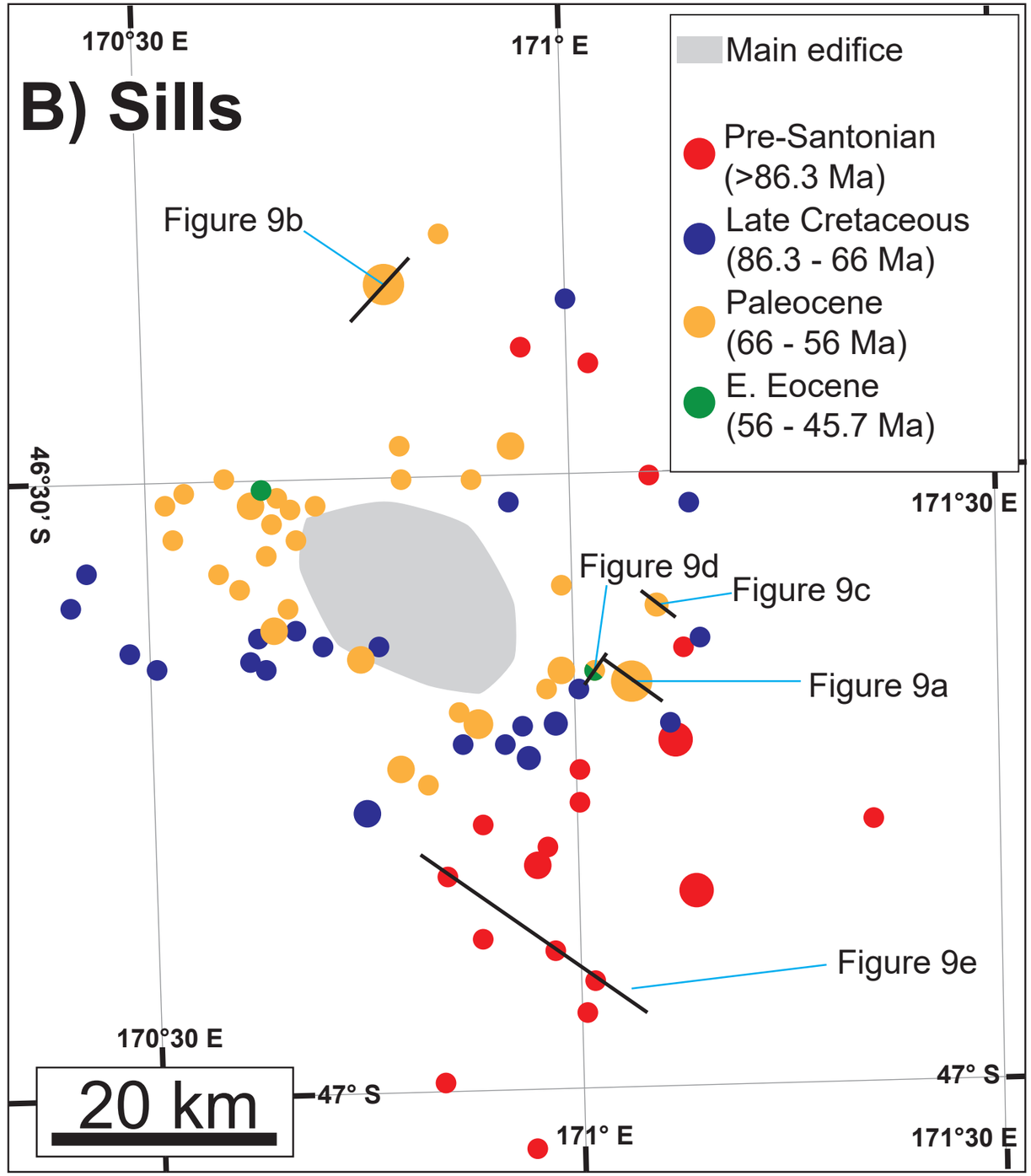
B) Sills
170°30 E
171° E
171°30 E
46°30' S
47° S
Main edifice
Pre-Santonian (>86.3 Ma)
Late Cretaceous (86.3 - 66 Ma)
Paleocene (66 - 56 Ma)
E. Eocene (56 - 45.7 Ma)
Figure 9b
Figure 9d
Figure 9c
Figure 9a
Figure 9e
20 km

Figure 7

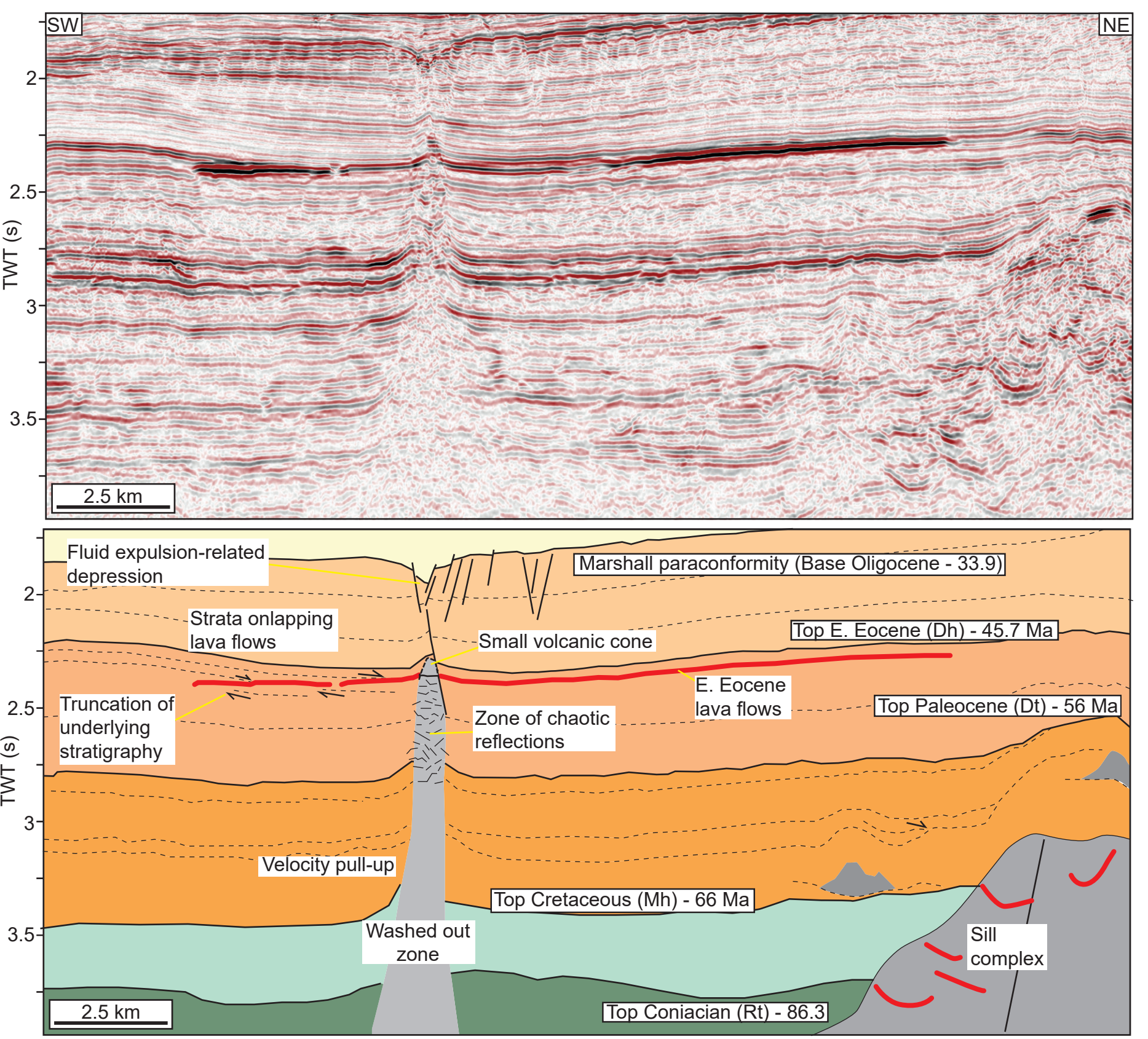
SW
NE
2
2.5
3
3.5
TWT (s)
2.5 km
Fluid expulsion-related depression
Marshall paraconformity (Base Oligocene - 33.9)
Strata onlapping lava flows
Small volcanic cone
Top E. Eocene (Dh) - 45.7 Ma
E. Eocene lava flows
Truncation of underlying stratigraphy
Zone of chaotic reflections
Top Paleocene (Dt) - 56 Ma
Velocity pull-up
Top Cretaceous (Mh) - 66 Ma
Washed out zone
Sill complex
Top Coniacian (Rt) - 86.3
2.5 km

Figure 8

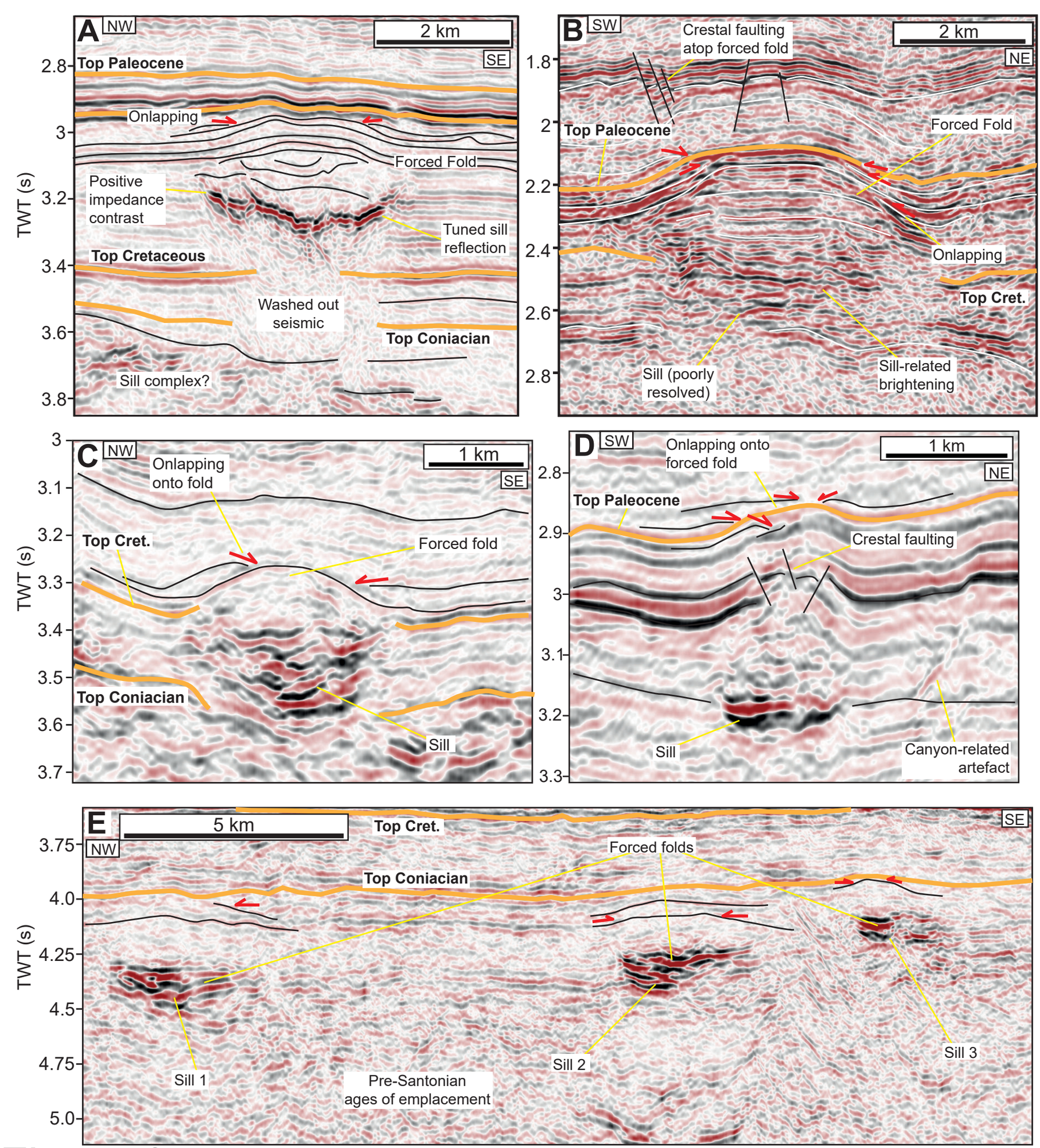
A
NW
SE
2 km
Top Paleocene
Onlapping
Forced Fold
Positive impedance contrast
Tuned sill reflection
Top Cretaceous
Washed out seismic
Top Coniacian
Sill complex?
TWT (s)
B
SW
NE
2 km
Crestal faulting atop forced fold
Top Paleocene
Forced Fold
Onlapping
Top Cret.
Sill (poorly resolved)
Sill-related brightening
C
NW
SE
1 km
Onlapping onto fold
Top Cret.
Forced fold
Top Coniacian
Sill
D
SW
NE
1 km
Onlapping onto forced fold
Top Paleocene
Crestal faulting
Sill
Canyon-related artefact
E
NW
SE
5 km
Top Cret.
Forced folds
Top Coniacian
Sill 1
Pre-Santonian ages of emplacement
Sill 2
Sill 3

Figure 9

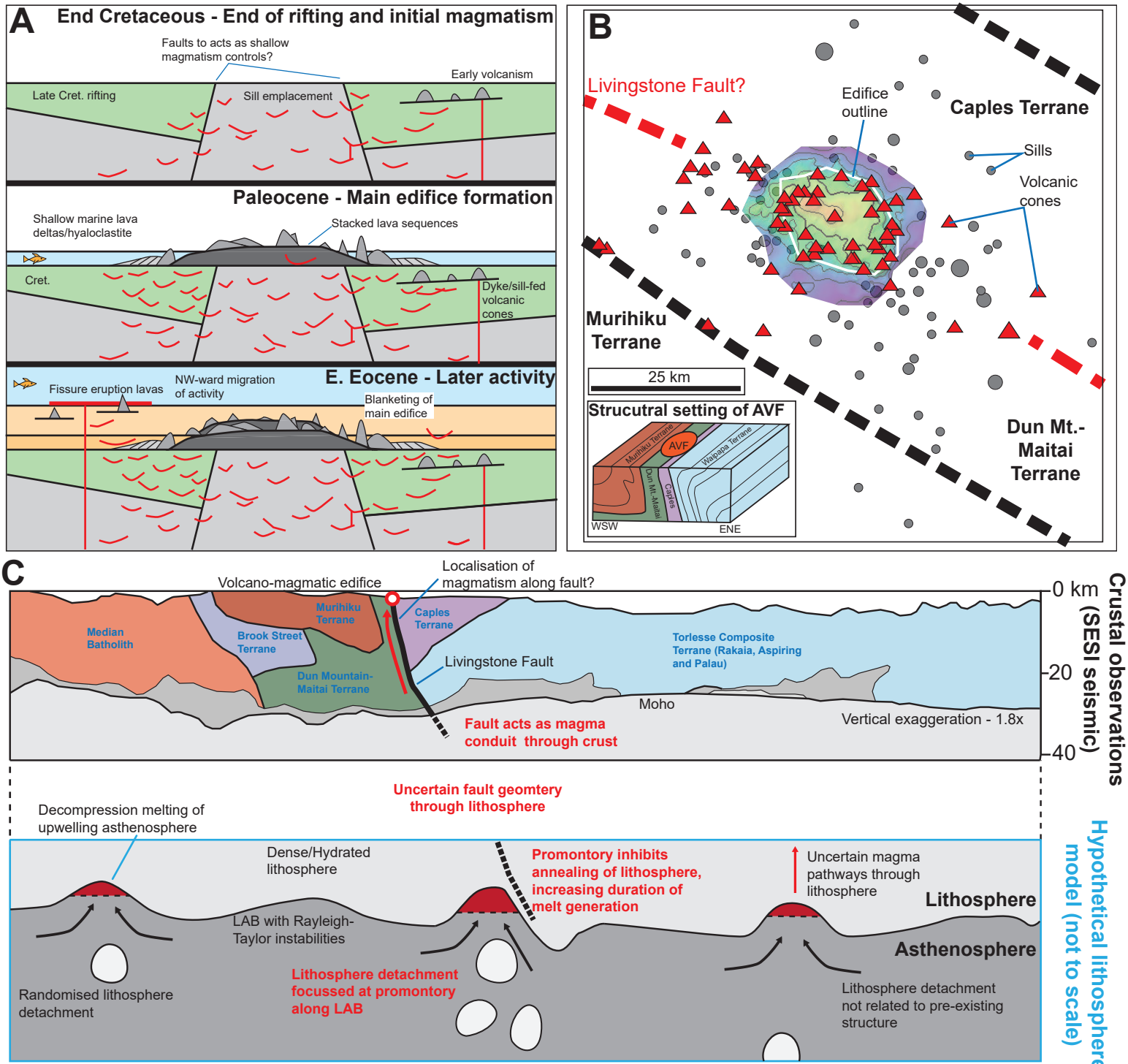
A
End Cretaceous - End of rifting and initial magmatism
Faults to acts as shallow magmatism controls?
Early volcanism
Late Cret. rifting
Sill emplacement
Paleocene - Main edifice formation
Shallow marine lava deltas/hyaloclastite
Stacked lava sequences
Cret.
Dyke/sill-fed volcanic cones
E. Eocene - Later activity
Fissure eruption lavas
NW-ward migration of activity
Blanketing of main edifice
B
Livingstone Fault?
Edifice outline
Caples Terrane
Sills
Volcanic cones
Murihiku Terrane
Dun Mt.-Maitai Terrane
25 km
Strucutral setting of AVF
Murihiku Terrane
AVF
Waipapa Terrane
Dun Mt.-Maitai
Caples
WSW
ENE
C
Volcano-magmatic edifice
Localisation of magmatism along fault?
Median Batholith
Brook Street Terrane
Murihiku Terrane
Caples Terrane
Dun Mountain-Maitai Terrane
Livingstone Fault
Torlesse Composite Terrane (Rakaia, Aspiring and Palau)
Moho
Fault acts as magma conduit through crust
Vertical exaggeration - 1.8x
0 km
20
40
Crustal observations (SESI seismic)
Uncertain fault geomtery through lithosphere
Decompression melting of upwelling asthenosphere
Dense/Hydrated lithosphere
Promontory inhibits annealing of lithosphere, increasing duration of melt generation
Uncertain magma pathways through lithosphere
Lithosphere
LAB with Rayleigh-Taylor instabilities
Asthenosphere
Lithosphere detachment focussed at promontory along LAB
Randomised lithosphere detachment
Lithosphere detachment not related to pre-existing structure
Hypothetical lithosphere model (not to scale)

Figure 10

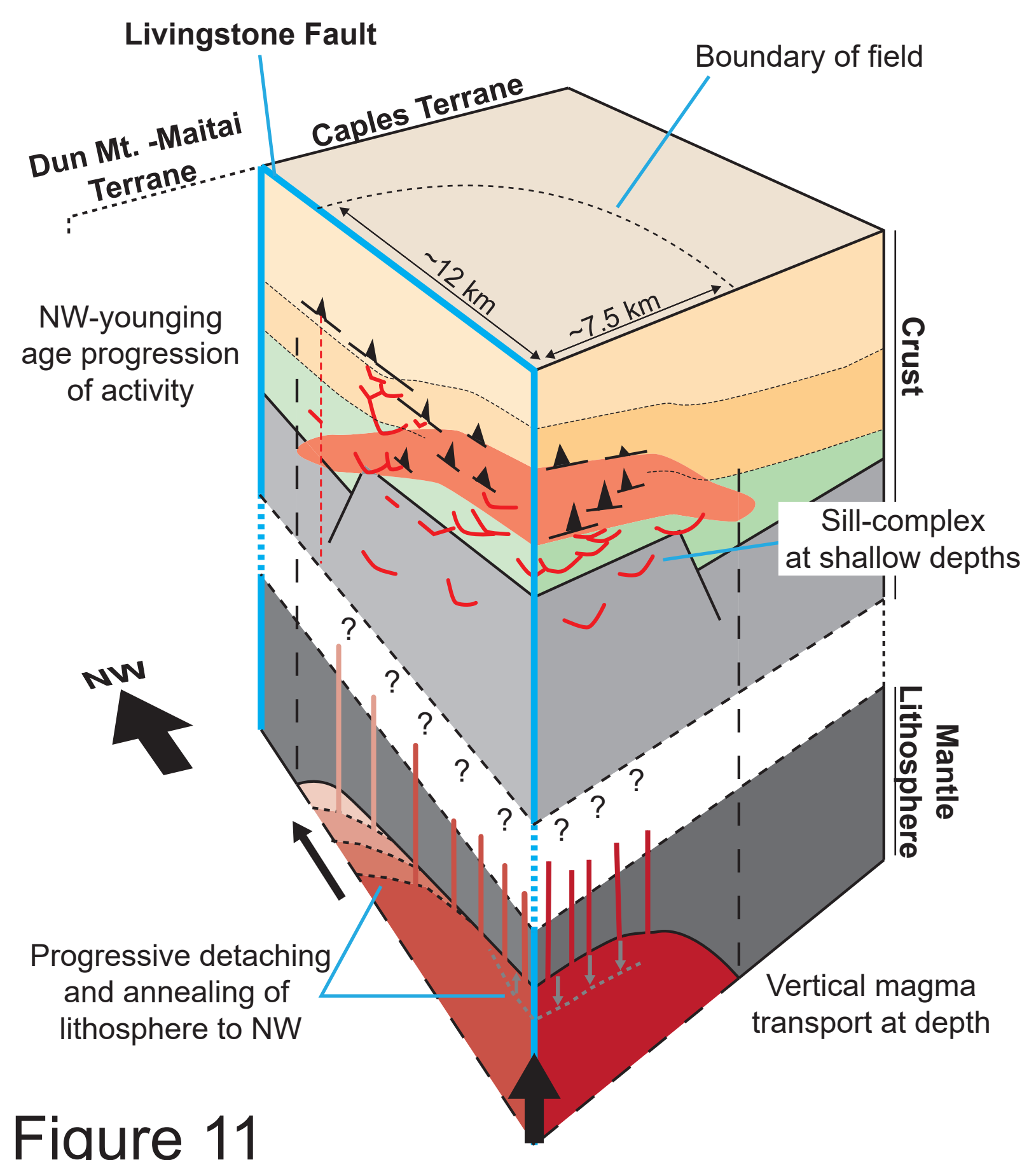
Livingstone Fault
Boundary of field
Caples Terrane
Dun Mt. -Maitai Terrane
~12 km
~7.5 km
NW-younging age progression of activity
Crust
Sill-complex at shallow depths
NW
Mantle Lithosphere
Progressive detaching and annealing of lithosphere to NW
Vertical magma transport at depth

Figure 11

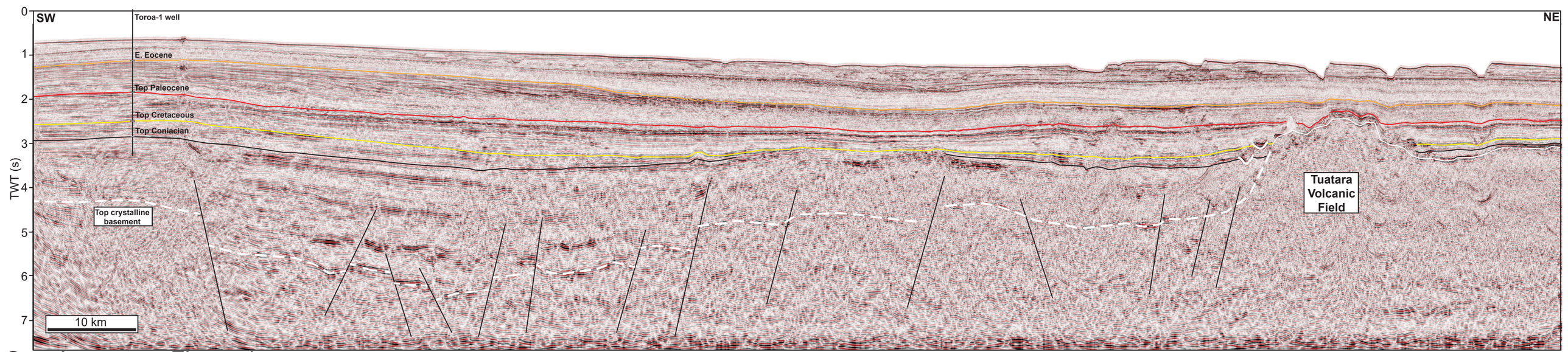

Supplementary Figure 1